



Universidad Autónoma
de Madrid

Biblos-e Archivo
Repositorio Institucional UAM

Repositorio Institucional de la Universidad Autónoma de Madrid
<https://repositorio.uam.es>

Esta es la **versión de autor** del artículo publicado en:
This is an **author produced version** of a paper published in:

Advanced Functional Materials 28.24 (2018): 1705938

DOI: <https://doi.org/10.1002/adfm.201705938>

Copyright: © 2018 WILEY-VCH Verlag GmbH & Co. KGaA, Weinheim

El acceso a la versión del editor puede requerir la suscripción del recurso
Access to the published version may require subscription

DOI: 10.1002/ ((please add manuscript number))

Article type: Full Paper

Dual role of subphthalocyanine dyes for optical imaging and therapy of cancer

Eveline van de Winckel⁺, Marta Mascaraque⁺, Alicia Zamarrón, Ángeles Juarranz de la Fuente, Tomás Torres*, Andrés de la Escosura**

Dr. E. van de Winckel, Prof. T. Torres, Dr. A. de la Escosura,
Departamento de Química Orgánica, Universidad Autónoma de Madrid, Madrid 28049, Spain
E-mail: andres.delaescosura@uam.es, tomas.torres@uam.es

M. Mascaraque, Dr. A. Zamarrón, Prof. A. Juarranz de la Fuente
Departamento de Biología, Universidad Autónoma de Madrid, Madrid 28049, Spain
E-mail: angeles.juarranz@uam.es

[+] These authors contributed equally to this work.

Keywords: subphthalocyanine dyes, optical imaging, photodynamic therapy, cancer

Abstract

The family of subphthalocyanine (SubPc) macrocycles represents an interesting class of non-planar aromatic dyes with promising features for energy conversion and optoelectronics. The use of SubPcs in biomedical research is, on the contrary, clearly underexplored, despite their documented high fluorescence and singlet oxygen quantum yields. Herein, we show for the first time that the interaction of these chromophores with light can also be useful for theranostic applications, which in the case of SubPcs comprise optical imaging and photodynamic therapy (PDT). In particular, the article evaluates, through a complete *in vitro* study, the dual-role capacity of a novel series of SubPcs as fluorescent probes and PDT agents, where the macrocycle axial substitution determines their biological activity. The 2D and 3D imaging of various cancer cell lines (i.e., HeLa, SCC-13 and A431) has revealed, for example, different subcellular localization of the studied photosensitizers (PS), depending on the axial substituent they bear. Our results also show excellent photocytotoxicities, which are affected by the PS localization. With the best dual-role PS, preliminary *in vivo* studies have demonstrated their therapeutic potential. Overall, the present paper sets the bases for an unprecedented biomedical use of these well-known optoelectronic materials.

1. Introduction

The integration of therapeutics and diagnostics, also called theranostics, represents a major goal of current biomedical research, which pursues to achieve more site-specific, efficient and personalized healthcare.^[1,2] A straightforward approach toward this goal involves the use of theranostic agents that comprise the therapeutic and diagnostic functions within a single molecular framework. Optical imaging and therapy methods are becoming indispensable in this respect, as they allow tuning both kinds of functions through designed interactions of the theranostic agent with light.^[3] Compared to other imaging modalities, fluorescence imaging presents various advantages such as its non-invasive character, subcellular spatial resolution, high temporal resolution, and high sensitivity in the detection of biological structures at low concentration levels.^[4] Photodynamic therapy (PDT),^[5] on the other hand, is a clinically approved form of phototherapy that makes use of nontoxic photoactive compounds, called photosensitizers (PS). When exposed selectively to light of a certain wavelength, PS become toxic to targeted malignant and other diseased cells or microorganisms,^[6] through the generation of singlet oxygen ($^1\text{O}_2$) and reactive oxygen species (ROS).^[7] Importantly, integrating fluorescence emission with the capacity to convert light into $^1\text{O}_2$ and ROS yields PS that can perform as both imaging and PDT agents.^[8,9] However, there are few examples of PS with optimum emission features for use as fluorescent probes, and vice versa. In this respect, herein we report for the first time on the promising dual-role of subphthalocyanine dyes for optical imaging and therapy of cancer.

Subphthalocyanines (SubPcs) form part of the pyrrolic macrocycle family, and comprise a $14-\pi$ electron aromatic structure with C_3 symmetry, formed by three isoindole units linked through aza bridges around a tetracoordinated boron atom.^[10] They are considered lower homologues of phthalocyanines (Pcs),^[11-15] which constitute one of the most important families of PS.^[16-21] In contrast to Pcs, SubPcs present a conical π surface, which renders

them with excellent properties for photovoltaic and optoelectronic applications,^[22] such as a lower tendency to aggregation and the possibility to tune them through axial substitution. Such features, in combination with the intense absorption and emission of SubPcs close to the therapeutic window (at ca. 560 and 570 nm, respectively), also enable their use in biomedical research, yet the number of reports about these non-planar chromophores in the context of fluorescence imaging^[23-25] or PDT^[26,27] remain extremely scarce. In this respect, both the well-known high SubPc fluorescence and ¹O₂ quantum yields ($\phi_F = 0.2-0.9$ and $\phi_\Delta = 0.5-0.7$, respectively)^[28-30] prompted us to explore the potential dual functioning of these dyes as fluorescent probes and PS for PDT.

The series of SubPc derivatives (**1a-c**, **Figure 1**) under study presents different substituents at the apical position of the boron atom, which allows tuning the balance between hydrophilicity and hydrophobicity of the PS. The design of the axial substituents in compounds **1a-c** is derived from a series of silicon Pc (SiPc) derivatives, bearing two of the same substituents at the axial positions of their silicon atom, described by some of us and which previously showed activatable photodynamic properties.^[31] These substituents include: (i) a bulky pyrene-containing hydrophobic group, where the pyrene moiety could be used as an additional fluorophore (**1a**); (ii) an amino group with two methoxy(triethylenoxy) axial chains for increasing hydrophilicity (**1b**); and (iii) a reference hydrophobic group that lacks the bulky pyrene unit (**1c**). Importantly, the rationale of the present study is to extend the interesting photodynamic activity of that SiPc-based series to compounds **1a-c**, where the SubPc platform provides an additional, outstanding potential for fluorescence imaging that Pcs just do not have. Consequently, we have developed an in-depth 2D and 3D *in vitro* study of SubPcs **1a-c** for fluorescence imaging of and PDT against HeLa, SCC-13 and A431 cancer cell lines. The selection of these cell lines is based on the fact that they all represent examples of superficial human cancers (cervix, skin and vulva, respectively) in which PDT can be

applied and, therefore, the type of lesions that could effectively be targeted by SubPcs without decreasing their activity due to tissue light absorption and scattering effects. Results from these studies show that the three PS derivatives (**1a**, **1b** and **1c**) are able to enter into these tumor cells, grown in monolayer (2D) or in spheroids (3D), inducing in both cases a strong fluorescence, in lysosomes or vacuoles (endosomes) depending on the SubPc axial substituent, under green light irradiation. Moreover, for the most efficient dual-role PS (**1a** and **1c**), preliminary *in vivo* studies in mice provide proof-of-concept of their promising therapeutic action.

2. Results and Discussion

2.1. Synthesis of SubPcs 1a-c

SubPcs **1a-c** were synthesized from SubPcBCl (**Scheme 1**), the synthesis of which was previously described.^[28] To allow for axial substitution with nucleophiles **2-4**,^[31] SubPcBCl was transformed into the reactive SubPc-triflate intermediate, following a successful substitution procedure developed previously in our research group.^[32] To this end, SubPcBCl was first dissolved in dry toluene and treated with 1.2 equiv. of silver triflate, to irreversibly remove the axial chlorine atom and to obtain a “SubPcB⁺” species with a weakly coordinating triflate anion. The formation of this triflate intermediate was followed by thin layer chromatography (TLC) and usually completes after ca. 40 min of reaction at room temperature. The activated SubPc-triflate intermediate shows considerable reactivity towards nucleophilic attack at the boron atom, and can be easily reacted with a variety of nucleophiles. Therefore, upon completion of the formation of the triflate intermediate, 2 equiv. of the corresponding nucleophile (i.e., compound **2**, **3** or **4**) were added to the reaction mixture, in the presence of 1.2 equiv. of freshly distilled DIPEA to neutralize the triflic acid generated in this step, which could promote unwanted side reactions. The reaction has to be performed

under strictly anhydrous conditions, as the presence of water traces immediately leads to a mixture of hydroxy-SubPc and the μ -oxo dimer.^[32] The resulting SubPcs **1a-c** could be easily purified by column chromatography, generally using toluene/THF mixtures of different polarities as the eluent. A second purification step by SEC, with Bio-Beads as the stationary phase and toluene as the eluent, was performed to remove any traces of free alcohol or μ -oxo dimer. In this way, SubPcs **1a-c** were obtained with moderate yields, ranging from 43% to 64% (see SI for the complete procedures).

2.2. Spectral features and photophysical properties

The normalized absorption spectra of SubPcs **1a-c**, measured in DMF (**Figure S1**), show the typical and intense Q band, at 566 nm for SubPcBCL and at 562 nm for the axially substituted SubPcs **1a-c**, which indicates that they are non-aggregated. Besides, they all present the typically broad Soret band, with a maximum around 305 nm. For SubPc **1a**, additional absorption bands at 329 and 345 nm can be distinguished, characteristic of the axial pyrene moiety. Exact values of the electronic absorption features for each SubPc can be found in **Table 1**. Upon excitation at 345 nm, all the SubPcs showed a fluorescence emission around 571 nm (F_{571}), varying in intensity, with the pyrene-bearing compound **1a** also showing a small emission band around 377 nm (F_{377}). The ϕ_F values for both the SubPc and pyrene moieties were determined in DMF, relative to F_{12} SubPcBCL in benzonitrile ($\phi_F = 0.58$) and anthracene in cyclohexane ($\phi_F = 0.36$), exciting at 520 nm or 345 nm, respectively (**Table 1**). As main conclusion, the ϕ_F of the three SubPcs **1a-c** were high (~ 0.3 - 0.6), encouraging their use for optical imaging. Besides, the emission of the pyrene unit from SubPc **1a** is quenched ($\phi_F = 0.02$), probably caused by an electronic energy transfer (EET) between the pyrene moiety and the SubPc core due to partial overlap of the pyrene emission spectrum with the

SubPc Q-band, yet electron transfer cannot in principle be ruled out.^[31] The photosensitizing efficiency of SubPcs **1a-c**, on the other hand, was evaluated by determining their ϕ_{Δ} in DMF following the well-known relative method, based on the photoinduced decomposition of the chemical scavenger 1,3-diphenylisobenzofuran (DPBF) (**Figure S2**), which reacts readily with $^1\text{O}_2$ (**Table 1**).^[33] From this data it can be inferred that the three SubPcs are efficient $^1\text{O}_2$ generators, with ϕ_{Δ} values between 0.37 and 0.56. The SubPc **1a** is a particularly good PS, equaling the photodynamic capacity of ZnPc, which was used as the reference compound.

2.3. Subcellular localization of SubPcs 1a-c

As the subcellular localization of a PS can determine its efficiency for PDT, as well as the type of cell death,^[34,35] the distribution of SubPcs **1a-c** within SCC-13 and HeLa cells was carefully evaluated by fluorescence microscopy, performing co-localization studies with fluorescent markers for specific organelles. To this end, cells were incubated for 18 h with SubPcs **1a-c** at a concentration of 2×10^{-6} M, and subsequently further incubated with LysoTracker[®], MitoTracker[®], or NBD C₆-ceramide probes. For both cell types, a similar intracellular distribution of SubPcs **1a-c** could be observed, as determined by their red fluorescence emission observed under green light excitation (**Figure 2** and **S3**). After incubation with SubPc **1a**, the two cell lines, grown in monolayer, showed an intense granular red fluorescence emission around the nucleus, as well as in a yuxtannuclear position (**Figure 2A left**). This intracellular emission of SubPc **1a** was coincident with that of the lysosomes, since a yellowish fluorescence due to the overlapping of red and green emission (from the SubPc and LysoTracker[®], respectively) was observed. Such fluorescence was clearly different from that of the mitochondrial and Golgi signal patterns. Identical results were obtained with SubPc **1b** (**Figure S3**). SubPc **1c**, on the contrary, showed a strong granular (vacuolar) red fluorescence emission localized also around the nucleus and nearby but not coincident with

lysosomes, neither with mitochondria nor with the Golgi apparatus (**Figure 2A right**). Control cells (without PS incubation) showed a very low emission, which corresponds to mitochondrial autofluorescence (not shown), confirming that the fluorescence detected in SCC-13 and HeLa was indeed due to intracellular accumulation of the SubPc dyes.

In addition, and taking into account that tumor spheroids are considered to be a better model to mimic the *in vivo* situation than monolayers of tumor cells, with regard to tumor shape,^[36,37] we then evaluated the ability of the SubPcs **1a-c** to penetrate into these tumor like structures formed from SCC-13 and HeLa cells (**Figure 2B**). As revealed by the intense emission observed under the fluorescence microscope, SubPcs **1a-c** effectively entered into the spheroids: SubPc **1a** localized in the lysosomes (identical localization was observed for SubPc **1b**, not shown), whereas SubPc **1c** presented a granular localization pattern nearby but not inside the lysosomes. From these observations, we can conclude that SubPcs **1a** and **1b** exhibit the same localization pattern in 2D and 3D *in vitro* localization experiments, both in SCC-13 and HeLa cells, being localized in lysosomes, whereas SubPc **1c** seems to present vacuolar (endosomal) localization. This is interesting because the subcellular localization of a PS is closely related to the cell death mechanism induced by PDT, as a consequence of the short life time of $^1\text{O}_2$, the main reactive species produced after PDT, for which the primary localization of the PS determines the initial subcellular damage upon its activation.^[38,39] Besides, given that no differences were detected between the SCC-13 and HeLa cells, localization seems to be mainly related to the molecular structure of the SubPc employed, for which repeating the subcellular localization experiments in A431 cells was considered not necessary.

2.4. Phototoxicity experiments and ROS production

The phototoxicity of SubPcs **1a-c** upon green light irradiation was evaluated by the MTT assay in SCC-13, HeLa and A431 cells, grown in monolayer. For this purpose, we first evaluated the inherent toxicity of two different concentrations of the three SubPcs (2×10^{-6} and 5×10^{-8} M) in cells after 5 h of incubation in presence of PS in the dark and, separately, in the absence of PS after the administration of different green light doses ($2 - 4.7 \text{ J/cm}^2$). The results obtained, shown in **Table 2**, indicate that none of these SubPc concentrations, neither the administration of green light, induced significant cytotoxic effects in the cell lines studied, and survival rates above 92% were obtained. We then continued to evaluate the photodynamic activity of the three SubPcs toward SCC-13, HeLa and A431 cells upon irradiation.^[40] For the photodynamic treatments, we selected the lower non-cytotoxic SubPc concentration (i.e., 5×10^{-8} M) and, after 5 h of incubation, cells were exposed to different green light doses (2, 3.35 and 4.7 J/cm^2). For both PDT treatments with SubPc **1a** and **1c**, a drastic decrease in cell survival was revealed for the three cell lines (**Figure 3 A-C**), in line with the light dose employed.

SubPc **1c** is a more efficient PS than **1a**, according to the statistically significant differences in performance observed between them. The measured cell survival values are actually comparable to those of other PS used in PDT, such as LDH-ZnPcS8,^[41] or silicaCe6-FA.^[42] SubPc **1b**, in turn, was not effective for PDT at this concentration, since the cell survival values obtained after photodynamic treatments were similar to those observed in untreated control cells. When higher concentrations of SubPc (i.e., 0.1×10^{-6} M) were employed, however, a significant decrease in cell survival was detected, even for SubPc **1b** (**Figure S4A**). Importantly, the observed cell survival values find correspondence to the capacity of the three SubPc dyes as $^1\text{O}_2$ generators (**Table 1**). Altogether, the results also indicate that HeLa cells were more resistant to photodynamic treatments with these SubPcs

than SCC-13 and A431 cells (**Figure S4B**). The cell morphology of the treated cells was also analyzed 24 h after PDT treatment using phase contrast microscopy (**Figure 3D**), revealing remarkable changes in the three cell lines. Most cells showed cytoplasmic retraction, with a rounded aspect similar to that of cells in apoptosis,^[43] yet elongated cells were also observed in the treated cultures. Interestingly, these images are well correlated with the results obtained from cell viability assays.

We next analysed by fluorescence microscopy the intracellular ROS formation in HeLa, SCC-13 and A431 cells, when subjected to PDT with the SubPc **1a** or **1c**, using for this purpose the DHF-DA fluorescent probe (**Figure S5**). As shown in **Figure S5A**, controls presented very low green fluorescent signal due to moderate endogenous production of ROS [44]. Similarly, cells incubated with SubPcs in dark conditions showed a very low green fluorescence. In contrast, cells subjected to PDT showed an intense fluorescence in all cell types, compared to baseline levels, revealing a prominent ROS production after the photodynamic treatment. Fluorescence values after PDT were actually significantly higher than for dark SubPc treatments ($P < 0.005$) (**Figure S5B**).

Given the results obtained in cells grown in monolayer, we next evaluated the photodynamic activity of SubPcs **1a** and **1c** in A431 spheroids. For the PDT treatments, we selected the highest non-cytotoxic SubPc concentration (2×10^{-6} M), 5 h of incubation, and a 4.7 J/cm^2 light dose. For both treatments, with SubPc derivatives **1a** and **1c**, a significant decrease in spheroid diameter can be observed 24h after treatment (**Figure 4A**). In addition, the acridine orange/ethidium bromide (AO/EB) staining method revealed that the treated spheroids were formed by damaged cells (fluorescing in orange/red) while controls were formed by viable cells (fluorescing in green) (**Figure 4B**). Therefore, we can conclude that both SubPcs were photodynamically active also in the 3D *in vitro* model.

2.5 *In vivo* studies

Preliminary *in-vivo* studies were performed to confirm the imaging and therapeutic potential of the SubPcs under study. As a proof of concept for imaging, we tested if it is possible to capture the fluorescence of these PS *in vivo*. In particular, 0.2 ml of 2×10^{-6} M SubPc in PBS buffer were injected subcutaneously on the back flank of a mice (CD-1, shaved of the back dorsal skin using a hair clipper), and the resulting fluorescence was immediately evaluated by the IVIS Lumina system ($\lambda_{exc} = 450$ nm, $\lambda_{em} = 580$ nm). Following this simple, non-optimized protocol, Figure S6 shows an image where the emission of compound **1a**, as an example, can be clearly identified (see white arrow), demonstrating that the fluorescence of SubPc dyes can be detected *in vivo*, and the skin is not a barrier to observe the compound.

To evaluate the therapeutic capacity of SubPcs **1a** and **1c**, on the other hand, A431 cells were subcutaneously injected in both flanks of mice and when the tumors reached a size between 5-7 mm of diameter, treatments were applied. No evident differences were observed in the size of tumors exposed only to light or with injected SubPc **1a** or **1c** (non-irradiated); therefore, all were grouped and shown as “controls”. For PDT treatments, the SubPcs **1a** or **1c** were administered by intratumoral injection and, 2 h later, exposed to 12 J/cm^2 of green light (**Figure 5A**). Treated tumors showed a size smaller than that of controls, as could be observed by visual inspection (**Figure 5B**) and confirmed after measuring them (**Figure 5C**). Reduction in tumor size was observed already 2 days after treatment, compared to controls not subjected to PDT. Tumors were subjected to a second PDT treatment and a greater decrease in their sizes was detected. The histological analysis of the tumors revealed no differences between the tumors with one or two PDT-treatments (not shown). The H&E staining showed an increment of red blood cell extravasation with progression to coagulative epidermal necrosis in tumors after SubPc injection and PDT (**Figure 5D**), this being related to the observed

smaller size of treated tumors. Therefore, both SubPcs are able to damage tumors cells upon green light irradiation.

3. Conclusions

In sum, in this article we have demonstrated for the first time, with *in vitro* and *in vivo* experiments, that SubPcs present a promising dual potential for optical imaging and photodynamic therapy of superficial cancers. This opens a window of opportunity for these optoelectronic dyes, whose application in biomedical research has, until now, remained clearly underexplored. The main advantages of SubPcs in this respect include their high fluorescence and singlet oxygen quantum yields, and their non-planar aromatic structure, which allows fine-tuning of the aggregation and excited state properties of these macrocycles by adequately designed axial substitution. Within the series of compounds studied herein, for example, different subcellular localization can be observed and related to the different SubPc axial substituents, an effect that we tentatively ascribe to their different aggregation behaviour in the biological medium. Although the structure – property relationships for this family of PS has to be clarified in further studies, their excellent capacity to perform both imaging and therapeutic functions that are triggered only by light represents a very promising approach within the field of theranostics.

4. Experimental Section

Materials and methods. All reagents were used as purchased from commercial sources without further purification. Solvents were dried using standard techniques prior to use. The starting materials silicon phthalocyanine dichloride (SiPcCl₂), 1-pyrene butyric acid, 2-hydroxyethyl disulfide, triethylene glycol monomethyl ether, and 3-amino-1-propanol were commercially available. Nucleophiles **2**, **3** and **4** were previously synthesized.^[31]

General procedure for the axial substitution of SubPcBCl. SubPcBCl (0.08 g, 0.19 mmol) and silver triflate (0.06 g, 0.23 mmol) were dissolved in anhydrous toluene (3 mL) and the mixture was stirred at rt under argon atmosphere for 40 min until SubPcBCl was consumed. Once the SubPc-triflate intermediate is generated, the nucleophile R-OH (**2**, **3** or **4**) (0.38 mmol) and DIPEA (40 μ L, 0.23 mmol) were added. The mixture was stirred at 40°C until the reaction was completed. The solvent was removed by evaporation under reduced pressure and the product was directly purified by column chromatography on silica gel using mixtures of toluene and THF as the eluent. Further specific purification steps for each SubPc are detailed in the *Supporting Information*.

Cell cultures. For *in vitro* studies, we used the following human tumoral cell lines: SCC-13 (squamous cell carcinoma from face), HeLa (cervical adenocarcinoma) and A431 (squamous cell carcinoma from vulva). Cell lines were grown in DMEM (Dulbecco's modified Eagle's medium high glucose 1X) supplemented with 10% (v/v) fetal bovine serum (FBS), 50 units/ml penicillin, and 50 μ g/ml streptomycin, all from Thermo Fisher Scientific Inc. Cell cultures were performed under standard conditions of 5% CO₂, 95% of humidity and 37°C of temperature and propagated by trypsinizing cultures with 1 mM EDTA/0.25% Trypsin (w/v).

Spheroid cultures. Spheroids were grown from SCC-13, HeLa and A431 cells using specific medium containing DMEM/F12 (1:1) (F-12 Nutrient Mixture, Ham, Gibco), 2% B27 serum free supplement (17504-044, Gibco), 20 ng/ml EGF (E4269, Sigma), 0.4% bovine serum albumin (A7906, Sigma) and 4 μ g/ml insulin (41400-045, Gibco). The cells were plated at 15,000 cells/ml per well pre-coated with 1.2% poly-HEMA (2-hydroxyethyl methacrylate, Sigma). The spheroids were formed after 6 days of culture.

Photosensitizer incubation. Stock solutions of the SubPcs **1a-c** (1.5×10^{-3} M) were prepared in DMSO and work solutions were obtained in DMEM without FBS. The final concentration of DMSO was always lower than 0.5% (v/v) and the lack of toxicity of such concentration for the cells was confirmed. All the treatments were performed when cultures reached around 60-70% of confluence.

Subcellular localization. To analyze the intracellular localization of SubPcs, SCC-13 and HeLa cells were grown on coverslips and, incubated with SubPcs **1a-c** to a final concentration of 2×10^{-6} M for 18 h at 37°C. After incubation, cells were further incubated for another 30 min with known fluorescent probes for lysosomes (LysoTracker[®] Green DND-26, Invitrogen), mitochondria (MitoTracker[®] Green FM, Invitrogen) or Golgi apparatus (NBD, C₆-ceramide (N-[6-[(7-nitro-2-1,3-benzoxadiazol-4-yl)amino]hexanoyl]-D-erythro-sphingosine, Invitrogen)) at the concentrations indicated by the suppliers. Then, cells were briefly washed in PBS, mounted on slides with a drop of PBS and immediately observed under the fluorescence microscope.

Photodynamic treatment. Monolayers of SCC-13, HeLa and A431 cells grown in 24-well plates were incubated with different concentrations of SubPcs, ranging from 0.05×10^{-6} M to 2×10^{-6} M (in DMEM without FBS) for 5 h. Subsequently, cells were irradiated with a green light emitting diode source ($\lambda = 525$ nm, the irradiance at the cell culture position was 11.1 mW/cm²) for variable doses, ranging from 2 to 4.7 J/cm². After irradiation, cells were further incubated in complete medium at 37°C for 24 h until evaluation. Spheroids were also treated in the same conditions used for the monolayers. Dark control experiments were carried out in parallel, incubating the cells with the same concentrations of SubPcs, for 5 h in dark. In the same way, to test the effect of green light alone, cells were subjected to different light doses.

Measurement of intracellular ROS. The intracellular production of ROS in SCC-13, HeLa and A431 cells was evaluated as previously described.^[45] Cells were incubated with SubPc **1a** or **1c** (0.05×10^{-6} M) for 5 h, and in the last hour 2,7-dichloro-dihydrofluorescein diacetate (DHF-DA, Abcam) was added to the cultures, reaching a final concentration of 6 μ M. Afterwards, and without removing DHF-DA, cells were exposed to green light (3.35 J/cm^2) and immediately after irradiation analysed by fluorescence microscopy, under blue excitation light ($\lambda_{\text{exc}} = 436 \text{ nm}$). Corresponding controls were performed: cells incubated with DHF-DA without SubPcs nor exposed to green light, and cells incubated with SubPcs and DHF-DA but not exposed to green light. ROS production was quantified by using Image J after measuring green fluorescence.

Morphological Changes and Cellular Toxicity. Changes in general cell morphology after 24 h photodynamic treatments were analyzed by phase contrast microscopy. The toxicity of SubPcs on cells grown in monolayer was evaluated 24 h after photodynamic treatment by the MTT (3-(4, 5-dimethylthiazol-2-yl)- 2, 5-diphenyltetrazolium bromide, Sigma) assay. MTT solution (1 mg/ml) in PBS was diluted in DMEM (10% FBS) to a final concentration of 50 μ g/ml, added to each well and incubated at 37°C for 3 h. After incubation, the formazan crystals were dissolved in DMSO and the absorbance at 542 nm was measured by spectrophotometry (Espectra Fluor 4, Tecan). Cellular toxicity was expressed as cell survival percentage of control (cell survival (%) = (mean OD value of PDT-treated cells / mean OD value of control cells) x 100%). The cellular toxicity in spheroids was evaluated by measuring their diameters using the Image J software, and by using two fluorescent dyes that bind to cells) DNA, acridine orange (stain both live and dead cells in green) and ethidium bromide (stain only cells that have lost membrane integrity in red).^[46]

Tumor Xenograft study. For *in vivo* study, we used eight hairless athymic nude mice from 6-8 weeks (BALB/cByJ-Hfh11nu; Charles River). Monolayer cultures of A-431 cells were trypsinized, resuspended in PBS and 2×10^6 cells were subcutaneously injected in both, right and left flanks of the animals. Mice were monitored for the appearance of tumors and treated when they reached a size between 5-7 mm of diameter (calculated from caliper measurements). The tumors were distributed as follows: 4 control light; 2 SubPc **1a** (unirradiated); 2 SubPc **1c** (unirradiated); 4 SubPc **1a**-PDT; and 4 SubPc **1c**-PDT. For PDT treatments, mice received 0.2 ml of 2×10^{-6} M SubPc **1a** or **1c** by intratumoral injection, and 2 h later, animals were exposed to 12 J/cm^2 green light by using the emitting diode source situated at 5 cm from the back of the animals. Four mice (half of tumors of each condition) were sacrificed 24 h after the treatments and tumors fixed in neutral buffered formalin, included in paraffin, sectioned and stained with hematoxylin and eosin (H&E) for pathological analysis. A second PDT treatment (in the same conditions as the first one) was administered to the tumors. The mice were then sacrificed and the tumors harvested for the same pathological analysis.

Microscopy and Statistical Analysis. Microscopic observations were carried out using an Olympus BX61 epifluorescence microscope, equipped with a HBO 100W mercury lamp and the corresponding filter sets for fluorescence microscopy: blue (450–490 nm, exciting filter BP 490), and green (545 nm, exciting filter BP 545). Photographs were obtained with digital camera Olympus DP50 and processed using Adobe PhotoShop CS5 extended version 12.0 software (Adobe Systems Inc, USA). Data are expressed as the mean value \pm standard deviation (SD) of at least three independent experiments. The statistical significance was determined using one-way ANOVA followed by Tukey's Test. A p-value lower than 0.05 was considered as significant.

Supporting Information

Supporting Information is available from the Wiley Online Library or from the author, and includes a complete description of procedures for the synthesis and characterization of compounds **1a-c**.

Acknowledgements

The research leading to these results has received funding from the People Programme (Marie Curie Actions) of the European Union's Seventh Framework Program FP7-PEOPLE-2012-ITN under REA grant agreement n° GA 316975. AdIE holds a Ramón y Cajal contract from the Spanish Ministry of Economy (MINECO). This work was supported by EU (CosmoPHOS-nano, FP7-NMP-2012-6, 310337-2; GLOBASOL, FP7-ENERGY-2012-J, 309194-2), the Spanish MINECO (CTQ-2014-52869-P (TT) and CTQ-2014-53673-P (AdIE)), CAM (FOTOCARBON, S2013/MIT-2841), grants from Instituto de Salud Carlos III, MINECO and Feder Funds (PI15/00974) and by S2010/BMD-2359 from Comunidad de Madrid.

Received: ((will be filled in by the editorial staff))

Revised: ((will be filled in by the editorial staff))

Published online: ((will be filled in by the editorial staff))

References

- [1] E. K. Lim, T. Kim, S. Paik, S. Haam, Y. M. Huh, K. Lee, *Chem. Rev.* **2015**, *115*, 327-394.
- [2] H. Chen, W. Zhang, G. Zhu, J. Xie, X. Chen, *Nat. Rev. Mat.* **2017**, *2*, 17024.
- [3] X. Ai, J. Mu, B. Xing, *Theranostics* **2016**, *6*, 2439-2457.

- [4] I. Johnson, in *Opt. Imaging Cancer*, Springer, New York, NY, **2010**, pp. 59–77.
- [5] M. H. Abdel-Kader, *Photodynamic Therapy - From Theory to Application*, Springer, **2014**.
- [6] M. Wainwright, T. Maisch, S. Nonell, K. Plaetzer, A. Almeida, G. P. Tegos, M. R. Hamblin, *Lancet Infect. Dis.* **2017**, *17*, e49-e55.
- [7] S. Nonell, C. Flors, *Singlet Oxygen: Applications in Biosciences and Nanosciences*, RSC Publishing, **2016**.
- [8] J. F. Lovell, T. W. B. Liu, J. Chen, G. Zheng, *Chem. Rev.* **2010**, *110*, 2839-2857.
- [9] M. Ethirajan, Y. Chen, P. Joshi, R. K. Pandey, *Chem. Sco. Rev.* **2011**, *40*, 340-362.
- [10] Christian G. Claessens, A. David González-Rodríguez, T. Torres, *Chem. Rev.* **2002**, *102*, 835–854.
- [11] J. A. A. W. Elemans, R. Van Hameren, R. J. M. Nolte, A. E. Rowan, *Adv. Mater.* **2006**, *18*, 1251–1266.
- [12] J. W. Ryan, E. Anaya-Plaza, A. de la Escosura, T. Torres, E. Palomares, *Chem. Commun.* **2012**, *48*, 6094-6096.
- [13] V. V. Roznyatovskiy, C.-H. Lee, J. L. Sessler, *Chem. Soc. Rev.* **2013**, *42*, 1921-1933.
- [14] H. Lu, N. Kobayashi, *Chem. Rev.* **2016**, *116*, 6184-6261.
- [15] T. Basova, A. Hassan, M. Durmus, A. G. Gürek, V. Ahsen, *Coord. Chem. Rev.* **2016**, *310*, 131–153.
- [16] N. Nishiyama, A. Iriyama, W.-D. Jang, K. Miyata, K. Itaka, Y. Inoue, H. Takahashi, Y. Yanagi, Y. Tamaki, H. Koyama, et al., *Nat. Mater.* **2005**, *4*, 934–941.
- [17] F. Dumoulin, M. Durmuş, V. Ahsen, T. Nyokong, *Coord. Chem. Rev.* **2010**, *254*, 2792–2847.
- [18] D. K. P. Ng, *Future Med. Chem.* **2014**, *6*, 1991-1993.
- [19] J. Mikkila, E. Anaya-Plaza, V. Liljestrom, J. R. Caston, T. Torres, A. de la Escosura,

- M. Kostianen, *ACS Nano* **2016**, *10*, 1565-1571.
- [20] J. A. Gonzalez-Delgado, P. J. Kennedy, M. Ferreira, J. P. C. Tome, B. Sarmento, *J. Med. Chem.* **2016**, *59*, 4428-4442.
- [21] E. Anaya-Plaza, E. van de Winckel, J. Mikkila, J.-M. Malho, O. Ikkala, O. Gulias, R. Bresoli-Obach, M. Agut, S. Nonell, T. Torres, M. A. Kostianen, A. de la Escosura, *Chem. Eur. J.* **2017**, *23*, 4320-4326.
- [22] C. G. Claessens, D. González-Rodríguez, M. S. Rodríguez-Morgade, A. Medina, T. Torres, *Chem. Rev.* **2014**, *114*, 2192–2277.
- [23] Y. Bernhard, P. Winckler, R. Chassagnon, P. Richard, É. Gigot, J.-M. Perrier-Cornet, R. A. Decréau, *Chem. Commun.* **2014**, *50*, 13975–8.
- [24] Y. Bernhard, P. Winckler, J.-M. Pierrer-Cornet, R. A. Decreau, *Dalton Trans.* **2015**, *44*, 3200-3208.
- [25] K. J. McAuliffe, M. A. Kaster, R. G. Szlag, E. R. Trivedi, *Int. J. Mol. Sci.* **2017**, *18*, 1177.
- [26] H. Xu, X.-J. Jiang, E. Y. M. Chan, W.-P. Fong, D. K. P. Ng, *Org. Biomol. Chem.* **2007**, *5*, 3987.
- [27] M. Spesia, E. Durantini, *Dye. Pigment.* **2008**, *77*, 229–237.
- [28] C. G. Claessens, D. González-Rodríguez, B. del Rey, T. Torres, G. Mark, H.-P. Schuchmann, C. von Sonntag, J. G. MacDonald, R. S. Nohr, *European J. Org. Chem.* **2003**, *14*, 2547–2551.
- [29] M. E. El-Khouly, A. El-Refaey, W. Nam, S. Fukuzumi, Ö. Göktuğ, M. Durmuş, L. Zhang, L. Ji, H. Liu, T. Torres, et al., *Photochem. Photobiol. Sci.* **2017**, *11*, 107–117.
- [30] N. Shibata, B. Das, E. Tokunaga, M. Shiro, N. Kobayashi, *Chem. Eur. J.* **2010**, *16*, 7554 – 7562.
- [31] E. van de Winckel, R. J. Schneider, A. de la Escosura, T. Torres, *Chem. A Eur. J.* **2015**,

- 21, 18551–18556.
- [32] J. Guilleme, D. González-Rodríguez, T. Torres, *Angew. Chemie Int. Ed.* **2011**, *50*, 3506–3509.
- [33] S. Makhseed, A. Tuhl, J. Samuel, P. Zimcik, N. Al-Awadi, V. Novakova, *Dye. Pigment.* **2012**, *95*, 351–357.
- [34] Y. J. Hsieh, C. C. Wu, C. J. Chang, J. S. Yu, *J. Cell. Physiol.* **2003**, *194*(3), 363-375.
- [35] J. J. Chen, L. J. Gao, T. J. Liu, *Oncol. lett.* **2016**, *11*(1), 775-781.
- [36] W. Mueller-Klieser, *Am. J. Physiol., Cell Physiol.* **1997**, *273*(4), C1109-C1123.
- [37] T. B. Andersson, *Basic Clin. Pharmacol. Toxicol.* **2017**.
- [38] J. Xu, F. Zeng, H. Wu, C. Hu, S. Wu, *Biomacromolecules.* **2014**, *15*(11), 4249-4259.
- [39] G. Kroemer, M. Jäättelä, *Nat. Rev. Cancer.* **2005**, *5*(11), 886-897.
- [40] L. B. de Paula, F. L. Primo, A. C. Tedesco, *Biophys. Rev.* **2017**, 1-13.
- [41] C. Li, B. Y. Zheng, M. R. Ke, Y. Zhang, J. D. Huang, J. Yoon, *Theranostics.* 2017 *7*(10), 2746-2756.
- [42] S. Bharathiraja, M. S. Moorthy, P. Manivasagan, H. Seo, K.D. Lee, J. Oh, *Photodiagnosis Photodyn. Ther.* **2017**, *19*, 212-220.
- [43] S. Rello, J. C. Stockert, V. Moreno, A. Gámez, M. Pacheco, A. Juarranz, M. Cañete, A. Villanueva, *Apoptosis.* **2005**, *10*(1), 201-208.
- [44] E. Carrasco, A. Blázquez-Castro, M. I. Calvo, A. Juarranz, J. Espada, *Methods* **2016**, *109*, 180-189.
- [45] A. Blázquez-Castro, E. Carrasco, M. I. Calvo, P. Jaén, J. C. Stockert, A. Juarranz, F. Sánchez-Rodríguez, J. Espada, *Cell Biol.* **2012**, *91*, 216-223.
- [46] S. Kasibhatla, G. P. Amarante-Mendes, D. Finucane, T. Brunner, E. Bossy-Wetzel, D. R. Green, *CSH Procols.* **2006**, (3), pdb-prot4493.

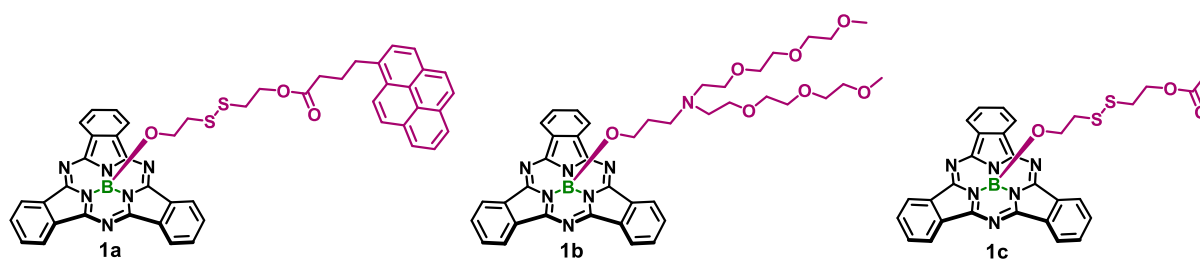
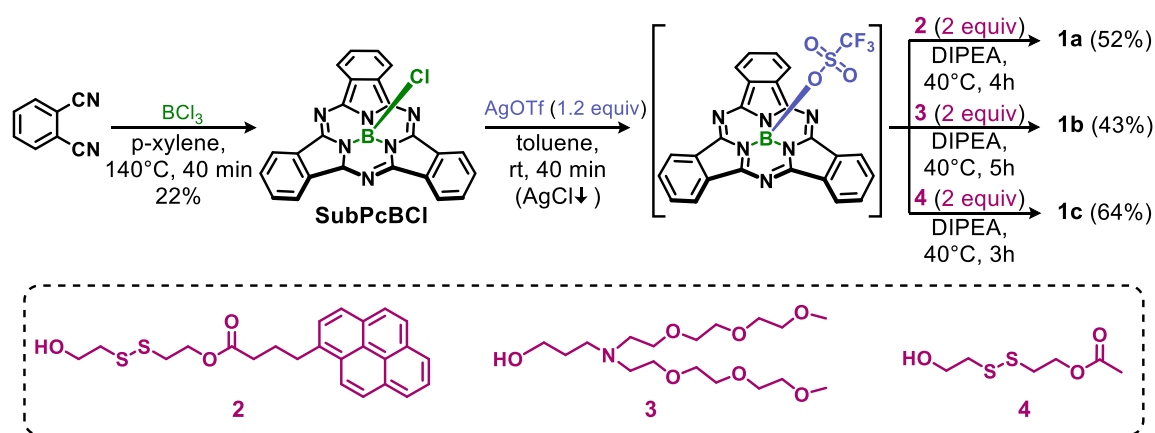


Figure 1. Chemical structure of the series of SubPc derivatives **1a-c**



Scheme 1. Scheme of the synthetic route toward SubPcs **1a-c**

Table 1. Electronic absorption and photophysical data for SubPcBCl and the SubPcs **1a-c** in DMF.

Compound	λ_{\max} [nm]	λ_{em} [nm] ^a	ϕ_{F377} [%] ^b	ϕ_{F571} [%] ^c	ϕ_{Δ} [%] ^d
SubPcBCl	566	575	- ^e	55	47
1a	562	571	2	38	56
1b	562	571	- ^e	29	37
1c	562	571	- ^e	36	49

^a) Excited at 520 nm. ^b) Excited at 345 nm, using anthracene in cyclohexane as the reference compound ($\phi_{\text{F}} = 0.36$). ^c) Excited at 520 nm, using F₁₂SubPcBCl in benzonitrile ($\phi_{\text{F}} = 0.58$) as the reference compound. ^d) Using ZnPc in DMF as the reference compound ($\phi_{\Delta} = 0.56$). ^e) Not applicable, because the compound does not contain any pyrene moiety.

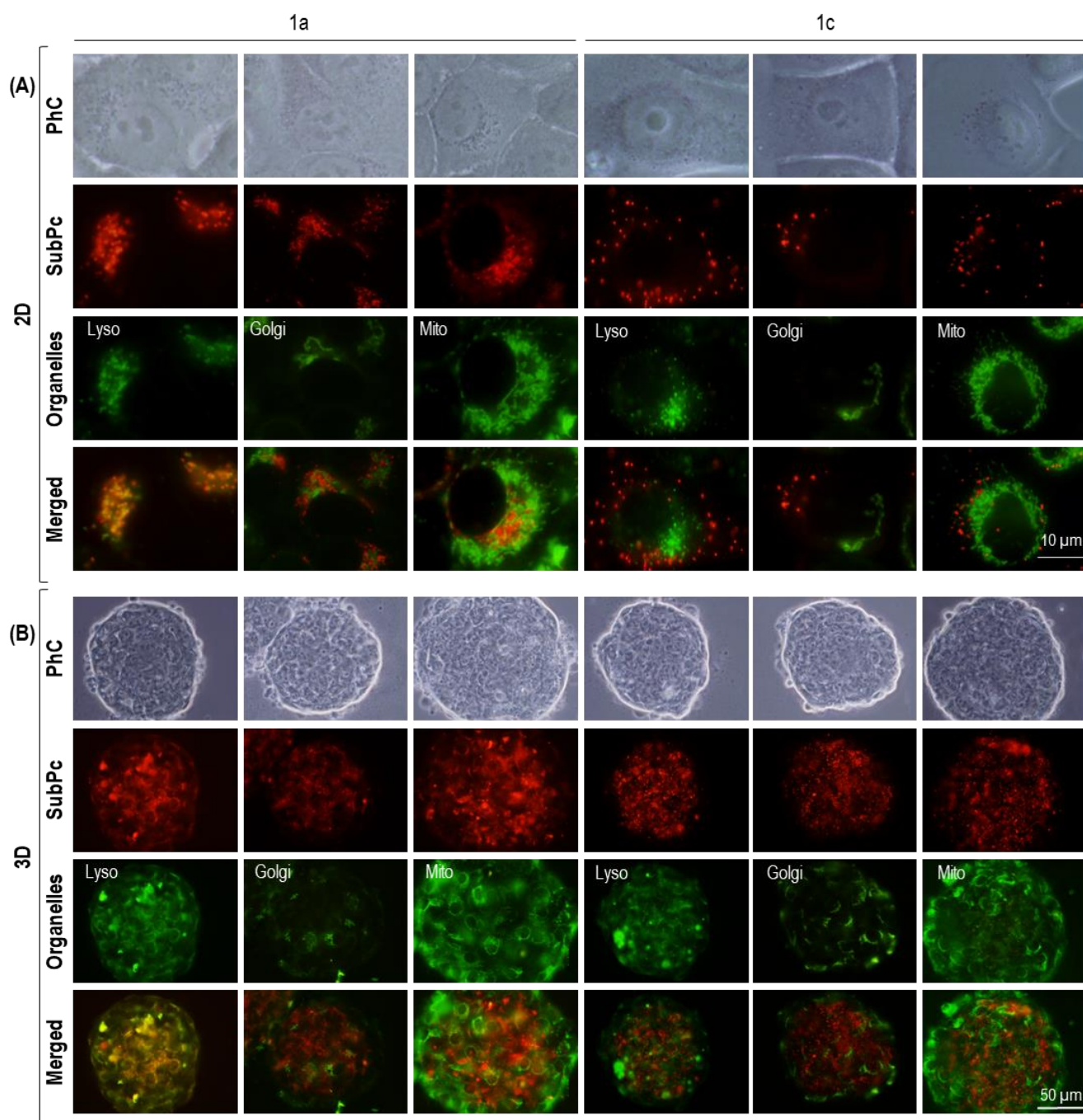


Figure 2. Subcellular localization of SubPc 1a and SubPc 1c in (A) 2D cultures and (B) 3D cultures of SCC-13 cells after 18 h of incubation. Experiments with cultures of HeLa cells gave identical results (not shown). Phase contrast (PhC). Red fluorescence is from SubPcs and green fluorescence is from lysosomes (Lyso), Golgi apparatus (Golgi) and mitochondrial (Mito). The merged image shows the green and red fluorescence together. A blue (450–490 nm) exciting lamp was used for LysoTracker[®] and MitoTracker[®] or NBD C₆-ceramide probes, while green (545 nm) exciting light was utilized for SubPcs.

Table 2. Toxicity effects in SCC-13, HeLa and A431 cells induced by green light, in the absence of any SubPc, and by incubation with SubPcs **1a-c** in the dark. Cell toxicity was evaluated by the MTT assay 24 h after treatment. Data are expressed as mean values obtained from three independent experiments \pm standard deviation (SD).

Compound	Concentration	Surviving fraction (% \pm SD)		
		SCC-13	HeLa	A431
Control		100 \pm 4.8	100 \pm 4.4	100 \pm 4.0
	4.7 J/cm ²	99 \pm 1.5	100 \pm 3.0	95 \pm 2.1
1a	2 x 10 ⁻⁶ M	101 \pm 3.6	102 \pm 4.7	95 \pm 2.0
	5 x 10 ⁻⁸ M	103 \pm 3.4	99 \pm 1.9	96 \pm 2.5
1b	2 x 10 ⁻⁶ M	102 \pm 4.6	104 \pm 1.5	103 \pm 1.1
	5 x 10 ⁻⁸ M	102 \pm 2.4	98 \pm 3.0	103 \pm 6.8
1c	2 x 10 ⁻⁶ M	95 \pm 2.9	96 \pm 2.9	92 \pm 2.4
	5 x 10 ⁻⁸ M	100 \pm 1.5	98 \pm 3.5	94 \pm 1.0

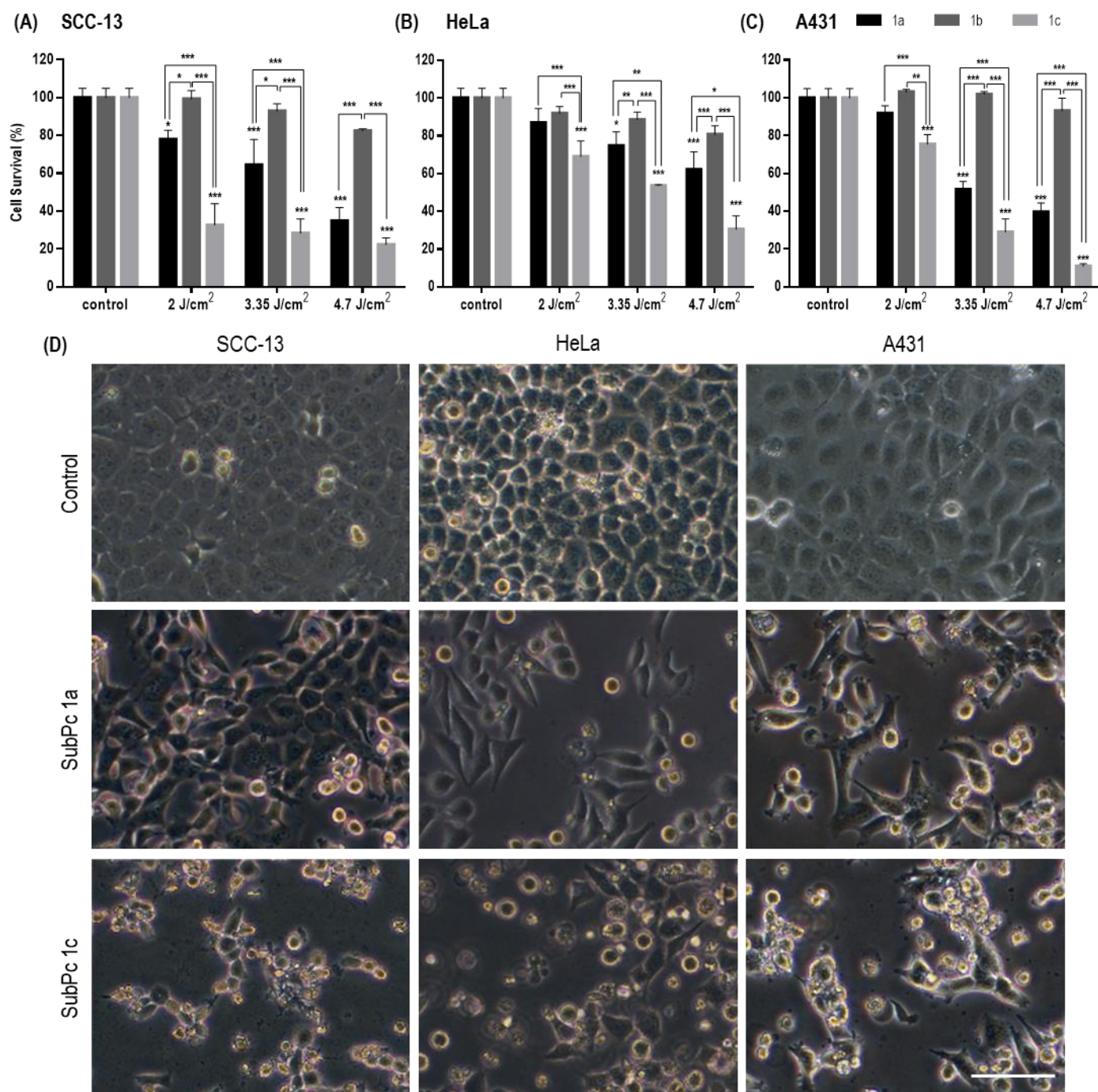


Figure 3. Survival of (A) SCC-13 (B) HeLa and (C) A431 cells after photodynamic treatment with SubPcs **1a-c** (5×10^{-8} M, 5 h of incubation followed by different light doses: 2, 3.35 and 4.7 J/cm²). Cell survival was evaluated 24 h after photodynamic treatment by the MTT assay. Each point corresponds to the mean value \pm SD obtained from three independent experiments. (D) Morphological changes observed in SCC-13, HeLa and A431 cells 24 h after PDT with the SubPcs **1a** and **1c** (0.05×10^{-6} M, 5 h of incubation followed by a green light dose of 4.7 J/cm²). Scale bar: 50 μ m. *P<0.05, **P<0.01, ***P<0.005.

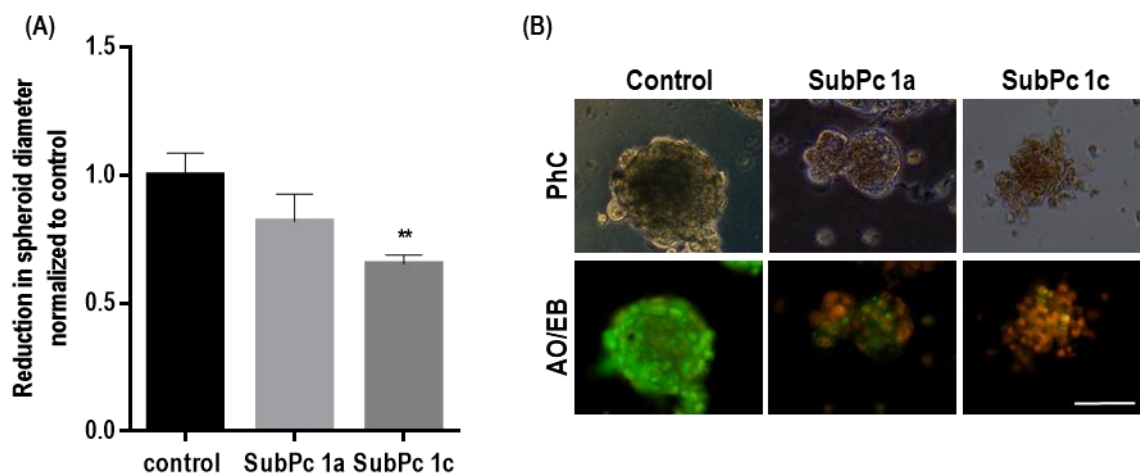


Figure 4. Photodynamic activity of SubPc **1a** and **1c** in A431 spheroids. **(A)** Reduction in spheroid diameters 24 h after PDT treatment with SubPcs **1a** and **c** (2×10^{-6} M, 5 h of incubation and 4.7 J/cm^2 of green light). Diameters were measured using the Image J software and normalized to size control. Each point corresponds to the mean value \pm SD obtained from three independent experiments. **(B)** 24 h after photodynamic treatment the spheroids were labelled with acridine orange (AO) and ethidium bromide (EB) to determine viable (green) or damage spheroids (orange). Scale bar: 50 μm . ** $P < 0.01$

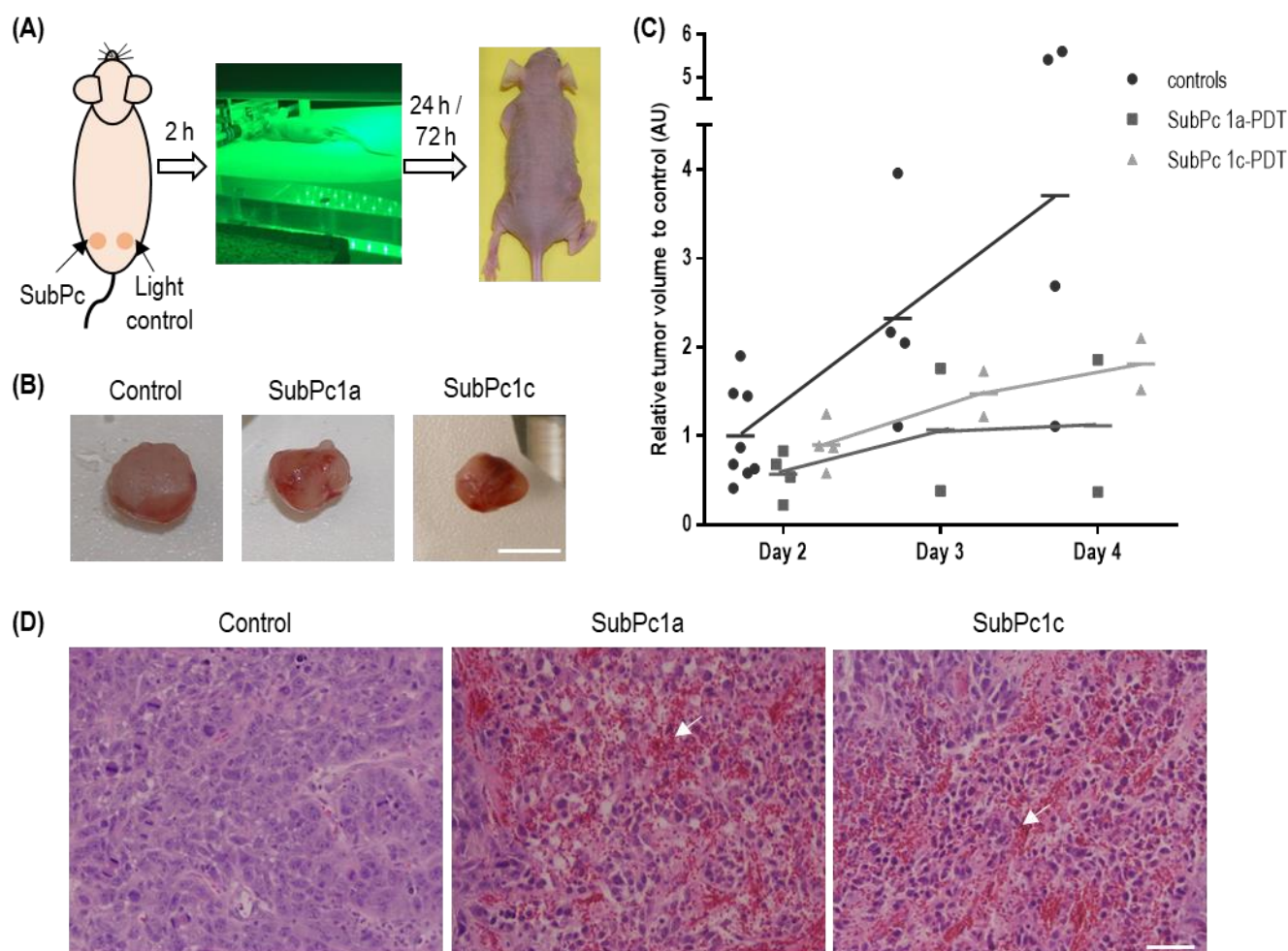


Figure 5. *In vivo* studies. (A) A-431 cells were injected in both right and left flanks of athymic nude mice. When the tumors reached a size between 5-7 mm of diameter, the tumors received 0.2 ml of 2×10^{-6} M SubPc **1a** or **1c** by intratumoral injection and, 2 h later, they were exposed to green light with a dose of 12 J/cm². (B) Representative tumors of each group (control, SubPc **1a**-PDT and SubPc **1c**-PDT), four days after the first PDT treatment. (C) Tumor volume to relative to control. Each point represents the volume of each tumor calculated as $\frac{4}{3}\pi \times (\text{diameter}/2)^3$. (D) Representative photographs of tumor sections stained with H&E 4 days after PDT treatments: control, SubPc **1a**-PDT and SubPc **1c**-PDT. Scale bar: 50 μm . Arrows indicate extravasated blood in the tumors as a result of SubPc-PDT treatments.

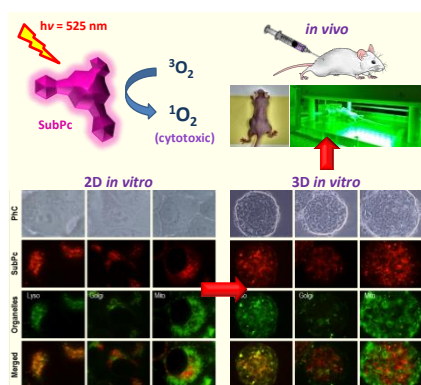
Table of Contents

The dual optical imaging and photodynamic therapy capacity of a series of SubPc photosensitizers bearing different axial substituents has been presented for the first time. The influence of the axial substituent on the subcellular localization and cell survival after photodynamic treatment has been carefully evaluated using 2D and 3D *in vitro* tumor models, and a proof of concept of *in vivo* therapeutic efficacy has been established in tumor-bearing mice.

Keywords: Subphthalocyanine dyes, optical imaging, photodynamic therapy, cancer

Eveline van de Winckel⁺, *Marta Mascaraque*⁺, *Alicia Zamarrón*, *Angeles Juarranz de la Fuente*^{*}, *Tomás Torres*^{*}, *Andrés de la Escosura*^{*}

Dual role of subphthalocyanine dyes for optical imaging and therapy of cancer



Supporting Information

Dual role of subphthalocyanine dyes for optical imaging and therapy of cancer

Eveline van de Winckel⁺, Marta Mascaraque⁺, Alicia Zamarrón, Ángeles Juarranz de la Fuente, Tomás Torres*, Andrés de la Escosura**

Table of Contents

- 1. Figures S1-S3**
- 2. Materials and Methods**
- 3. Synthesis and Characterization SubPcs 1a-c**
- 4. References**

1. Figures S1-S4

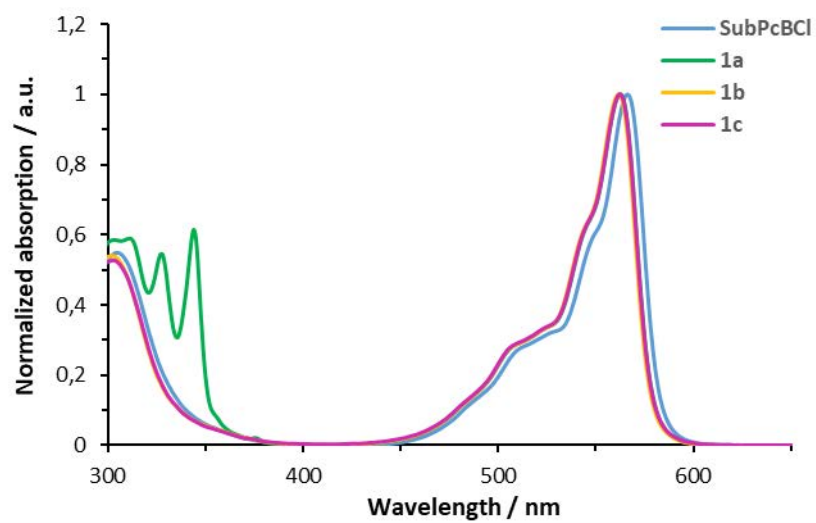


Figure S1. Electronic absorption spectra of SubPcBCL and the SubPcs **1a-c** in DMF.

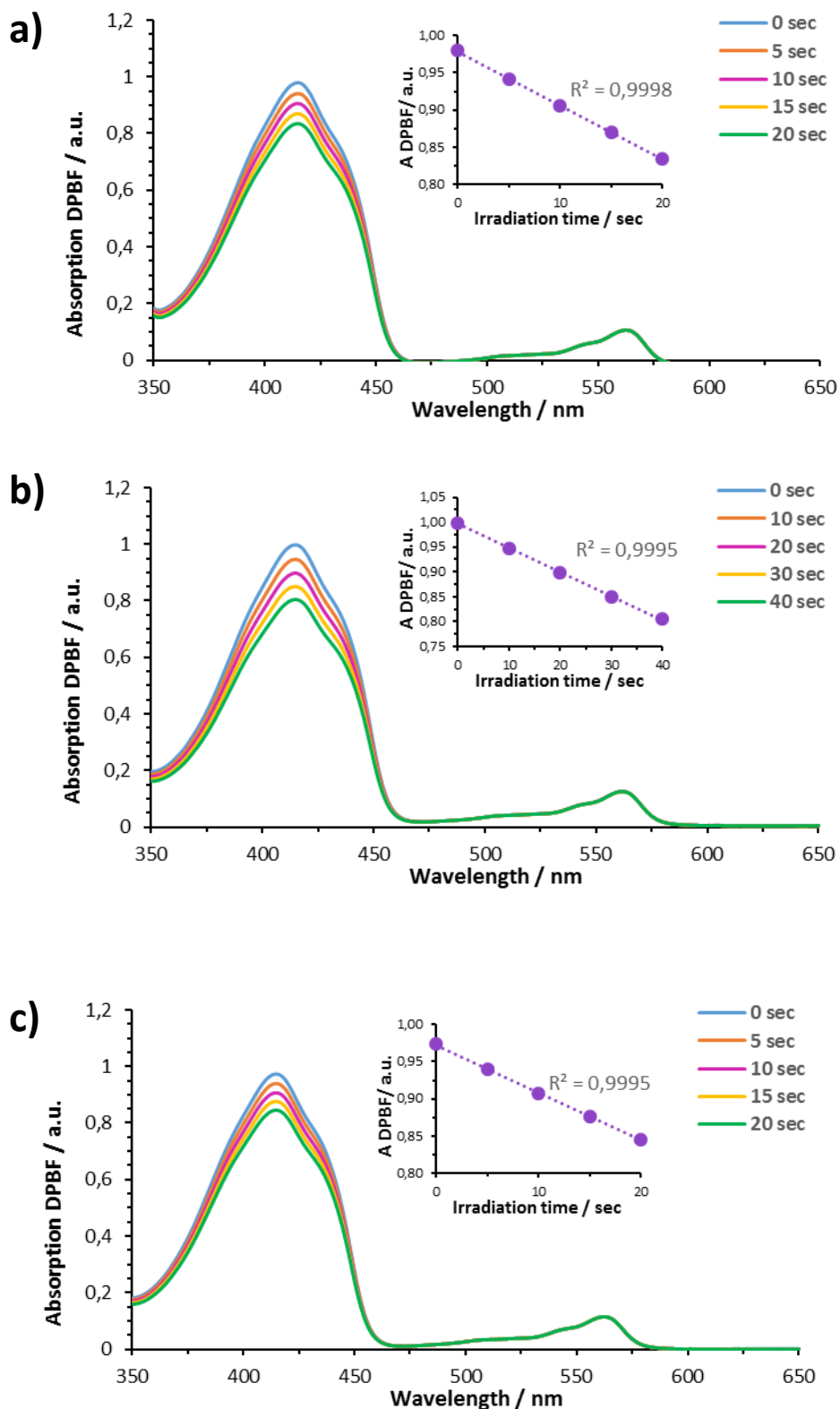


Figure S2. Singlet oxygen studies performed for the PS compounds **1a-c** in solution. In particular, the figure shows the plot of the DPBF $^1\text{O}_2$ scavenger absorption decay in DMF for the SubPcs (a) **1a**, (b) **1b** and (c) **1c**.

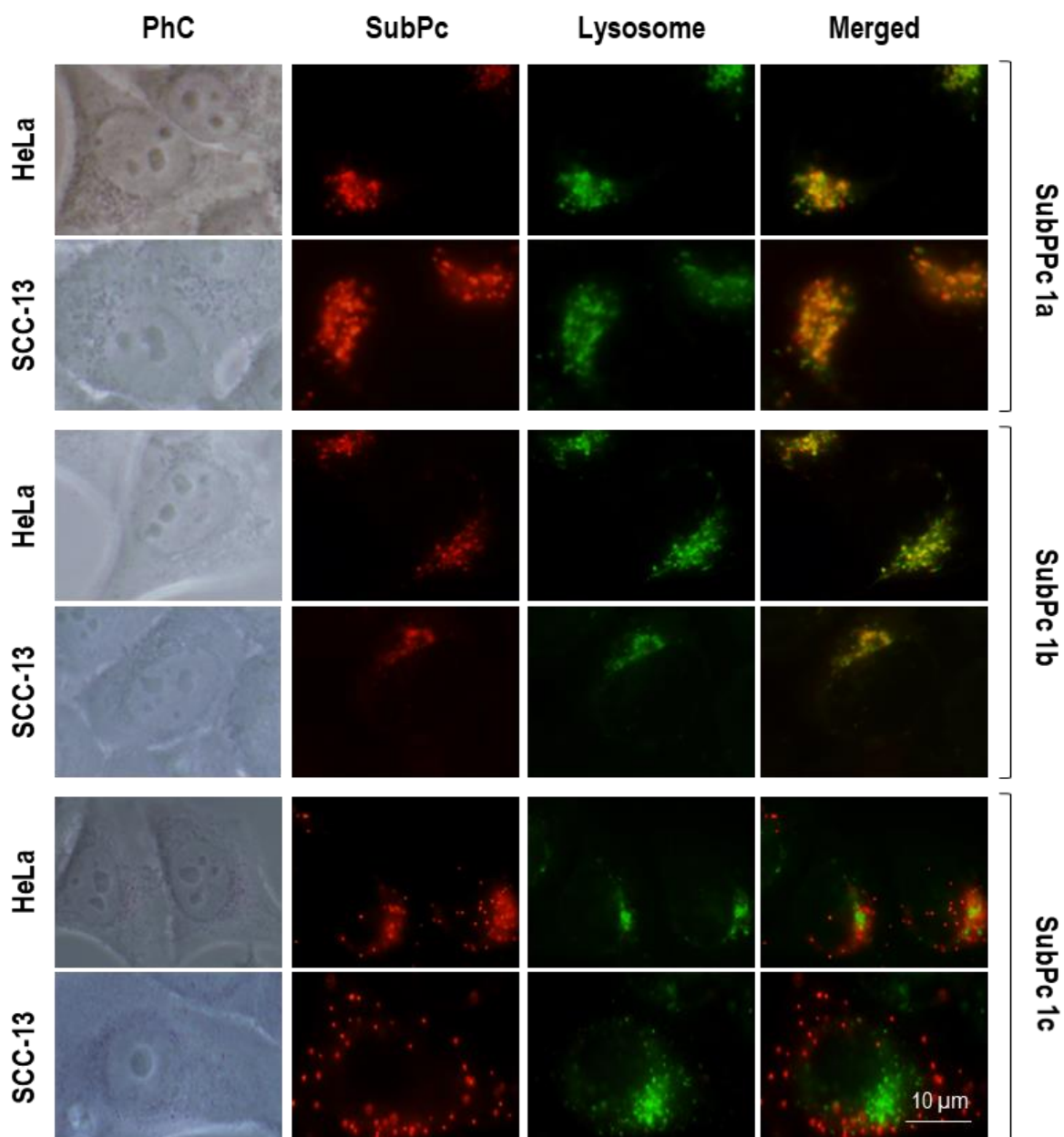


Figure S3. Subcellular localization of SubPc **1a-c** in HeLa and SCC-13 cells. Phase contrast (PhC). Red fluorescence corresponds to SubPcs and green fluorescence to lysosomes (labelled with LysoTracker[®]). The blue (450–490 nm) and green (545 nm) exciting lights were used for LysoTracker[®] or SubPcs, respectively.

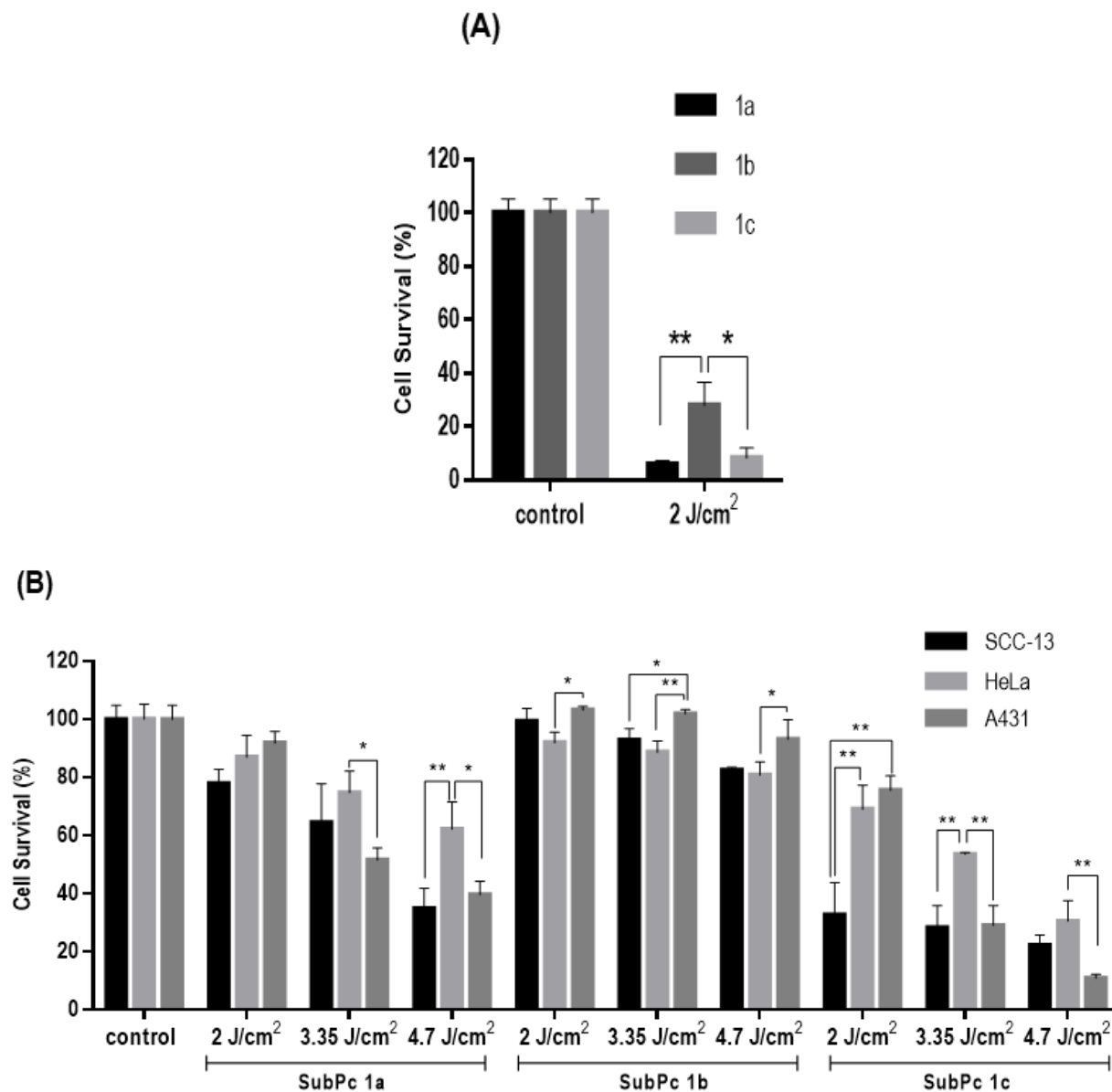


Figure S4. (A) Cell survival of HeLa cells after 5 h incubation with 0.1×10^{-6} M of SubPc followed by green light irradiation (2 J/cm^2). (B) Cell survival of SCC-13, HeLa and A431 cells after 5 h incubation with 5×10^{-8} M SubPc followed by different green light doses (2 , 3.35 and 4.7 J/cm^2). Cell survival was evaluated by the MTT assay 24 h after photodynamic treatments. Data on panels represent mean values from three independent experiments \pm SD. * $P < 0.05$, ** $P < 0.01$.

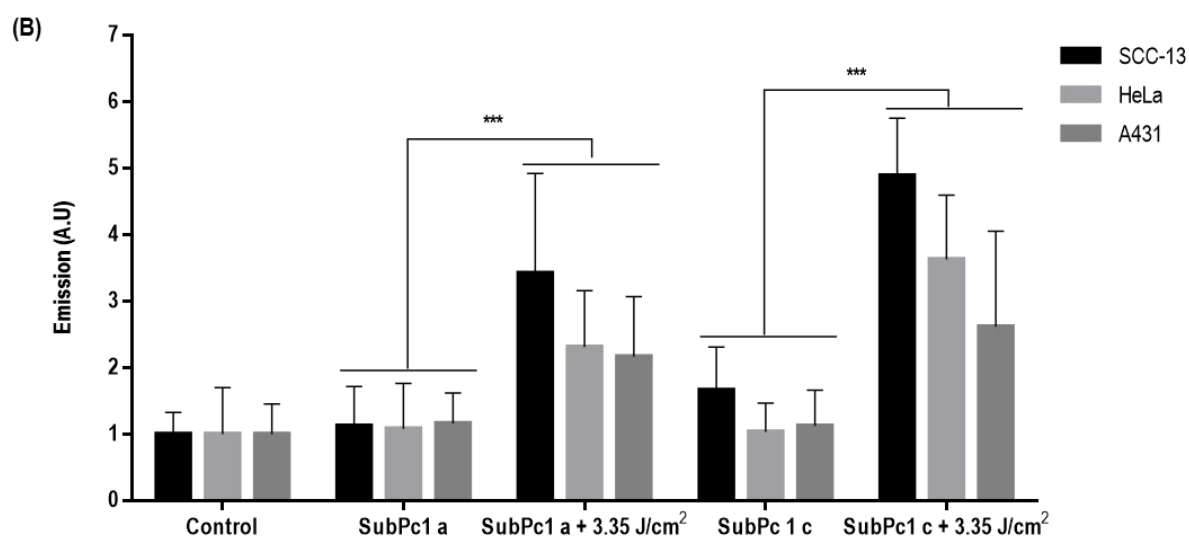
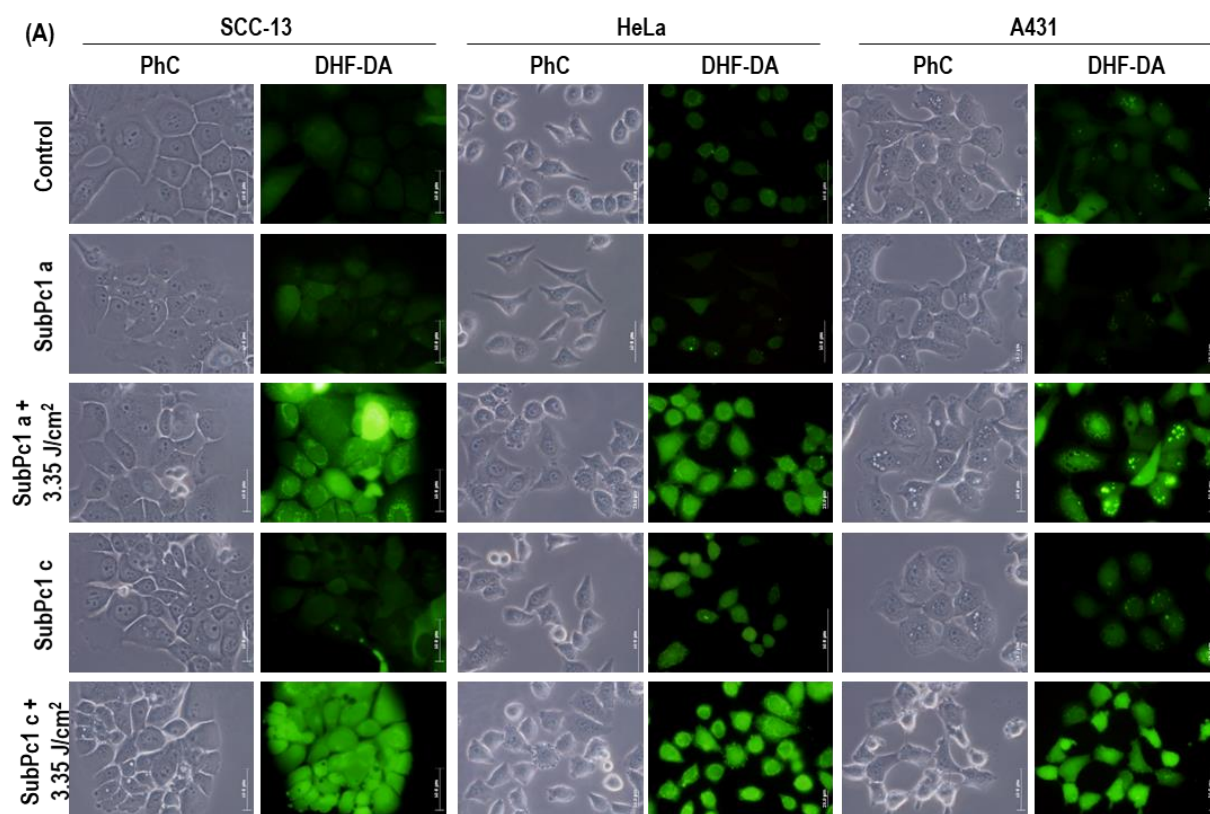


Figure S5. ROS production detected by the DHF-DA fluorescent probe after PDT with SubPcs **1a** or **1c** and green light. Cells were incubated with 0.05×10^{-6} M SubPc for 5 h, and in the last hour DHF-DA was added, reaching a final concentration of 6 μ M. Cells were exposed to green light (3.35 J/cm^2). The fluorescence signal was observed by using fluorescence microscopy ($\lambda_{\text{exc}} = 436 \text{ nm}$) (A). Intracellular fluorescence intensity was measured by ImageJ (B). *** $P < 0.005$.

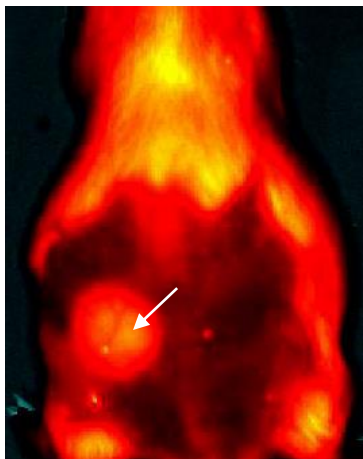


Figure S6. Image taken with the IVIS Lumina system ($\lambda_{exc} = 450 \text{ nm}$, $\lambda_{em} = 580 \text{ nm}$), showing the subcutaneous fluorescence of SubPc **1a** on the left back flank of a mice (CD-1, shaved of the back dorsal skin using a hair clipper), after injection of 2 mL of $2 \times 10^{-6} \text{ M}$ SubPc dye in PBS.

2. Materials and methods

All reactions were performed in standard glassware under inert argon atmosphere. Reactions were monitored by TLC, using TLC plates pre-coated with silica gel 60-F254 (Merck). Column chromatography was carried out on Merck silica gel 60, 40-63 μm (230-400 mesh). Size Exclusion Chromatography (SEC) was performed using Biorad Biobeads SX-1 (200-400 mesh). ^1H and $^{13}\text{C}\{^1\text{H}\}$ NMR spectra were recorded using Bruker AC-300 (^1H : 300 MHz; ^{13}C : 75 MHz) instruments, unless mentioned otherwise. Spectra were referenced internally by using the residual solvent (^1H : $\delta = 7.26$ for CDCl_3 , $\delta = 2.49$ for DMSO-d_6) or solvent resonances (^{13}C : $\delta = 77.0$ for CDCl_3 , $\delta = 39.5$ for DMSO-d_6) relative to SiMe_4 , respectively. UV-Vis and fluorescence spectra were recorded with a JASCO V-660 and a JACSO FP-8600 spectrophotometer, respectively. The logarithm of the molar absorption coefficient ϵ is expressed in between parentheses. Matrix-assisted laser desorption/ionization time of flight (MALDI-TOF) MS and high-resolution (HR-MS) mass spectra were recorded with a Bruker Ultrareflex III spectrometer. Fast atom bombardment (FAB) mass spectra were recorded with a VG AutoSpec of Waters instrument. All MS experiments were carried out at the Servicio Interdepartmental de Investigación (SIIdI) of the Universidad Autónoma de Madrid. All the data are expressed with the intensity in percentage between parentheses. IR spectra (IR) were recorded on a FT-IR Cary 630 (Agilent Technologies) using the ATR technique. Spectra intensity were corrected by ATR algorithm and subsequent baseline correction. Melting points (Mp) were determined in a Buchi 504392-S equipment, in the Department of Organic Chemistry of the Universidad Autónoma de Madrid.

Fluorescence quantum yields. ϕ_F values were measured in DMF using the comparative method of Williams et al,^[1] in which ϕ_F is determined by the equation:

$$\phi_F^S = \phi_F^R \left(\frac{Grad_S}{Grad_R} \right) \left(\frac{\eta_S^2}{\eta_R^2} \right)$$

where subscripts R and S denote reference and sample, respectively, ϕ_F is the fluorescence quantum yield, *Grad* the gradient from the plot of the integrated fluorescence intensity (at the specified wavelength) versus the absorption (at the same wavelength), and η the refractive index of the solvent. F₁₂SubPcBCl in benzonitrile ($\phi_F = 0.58$)^[2] and anthracene in cyclohexane ($\phi_F = 0.36$)^[3] were used as references for the SubPc and pyrene emissions, respectively. Excitation took place at 520 nm for SubPc and at 310 nm for pyrene moieties.

Singlet oxygen quantum yields. ϕ_Δ values were measured in DMF following the well-known relative method, based on the photoinduced decomposition of a chemical scavenger (i.e., DPBF) that reacts readily with ¹O₂.^[4] Non-substituted ZnPc was used as reference compound ($\phi_\Delta(\text{DMF}) = 0.56$).^[5] In detail, the procedure was as follows: 2.5 mL of a stock solution of DPBF (with an absorption of ca. 1) in DMF was transferred into a 10 x 10 mm quartz optical cell and bubbled with ³O₂ for 1 min. A concentrated stock solution of the SubPc in the same solvent was then added, in a defined amount to reach a final Q band absorbance value of about 0.1 au. The solution was stirred and irradiated for defined time intervals, using a halogen lamp (300 W). The duration of these intervals is tuned in each experiment, in order to get a decrease in DPBF absorption of about 3-4%. Incident light was filtered through a water filter (6 cm) and an additional filter to remove light under 455 nm (Newport filter 20CGA-455). Additional neutral density filters (FBS-ND03 or FB-ND10) were used when necessary. The decrease of DPBF absorbance with irradiation time was monitored at 414 nm. ϕ_Δ was calculated through the following equation:

$$\phi_{\Delta}^S = \phi_{\Delta}^R \frac{k^S I_{aT}^R}{k^R I_{aT}^S}$$

where R and S indicate reference and sample, respectively. k is the slope of a plot of $\ln(A_0/A_t)$ versus irradiation time t , with A_0 and A_t being the absorbance of scavenger at the monitoring wavelength before and after irradiation time t , respectively. I_{aT} is the total amount of light absorbed by the dye and is calculated as the sum of intensities of the absorbed light I_a from wavelength 530 up to 800 nm. I_a at given wavelength is calculated using Beer's law:

$$I_a = I_0(1 - e^{-2.3A})$$

where I_0 is the transmittance of the filter at a given wavelength and A the absorbance of the dye at this wavelength. All experiments are performed three times and the obtained data represent mean values of those three experiments.

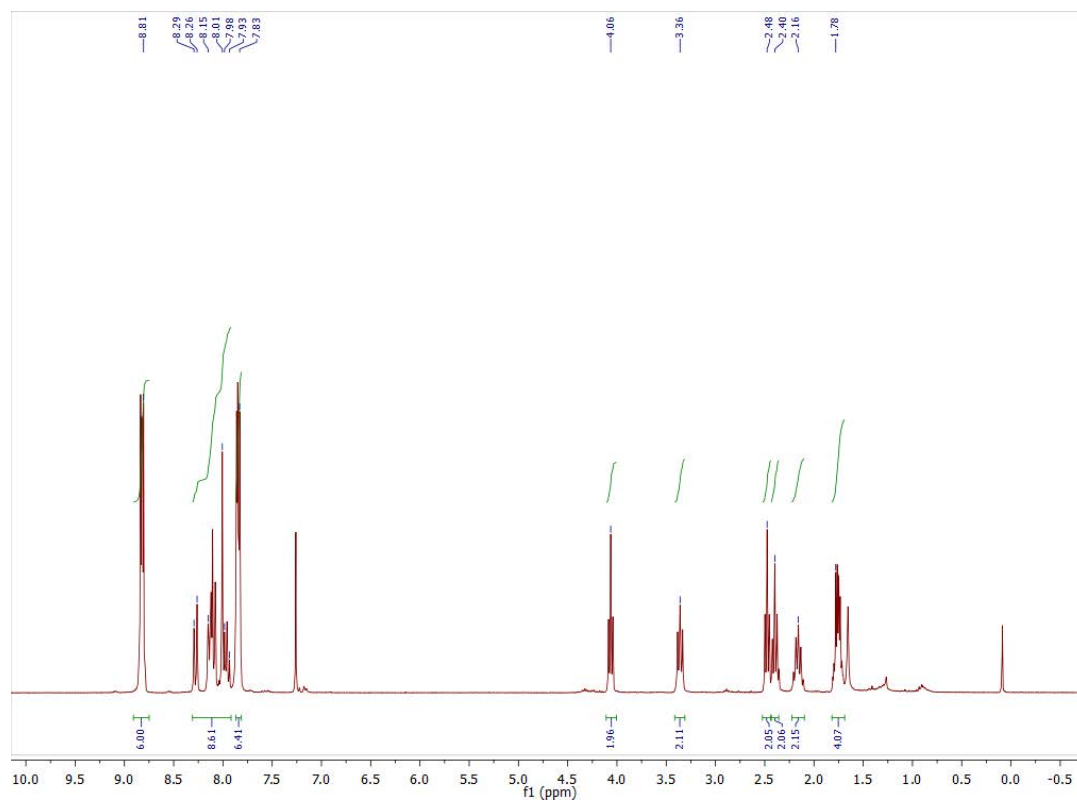
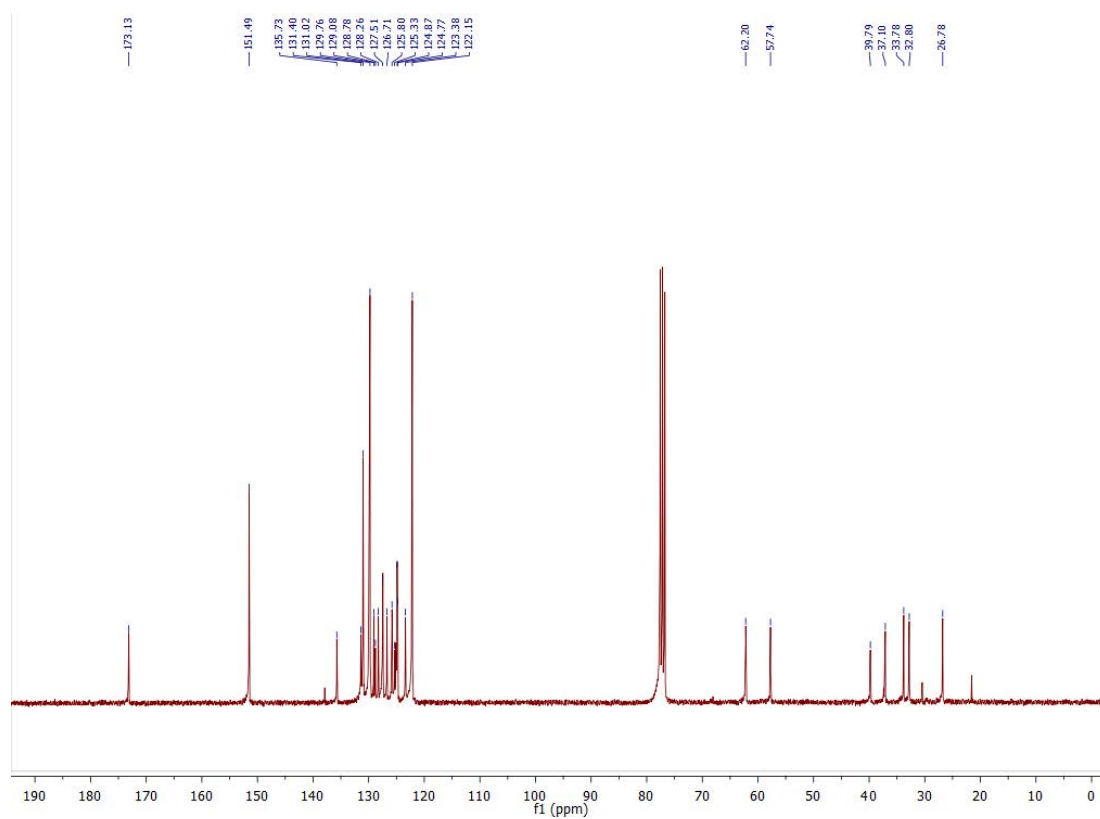
3. Synthesis and Characterization

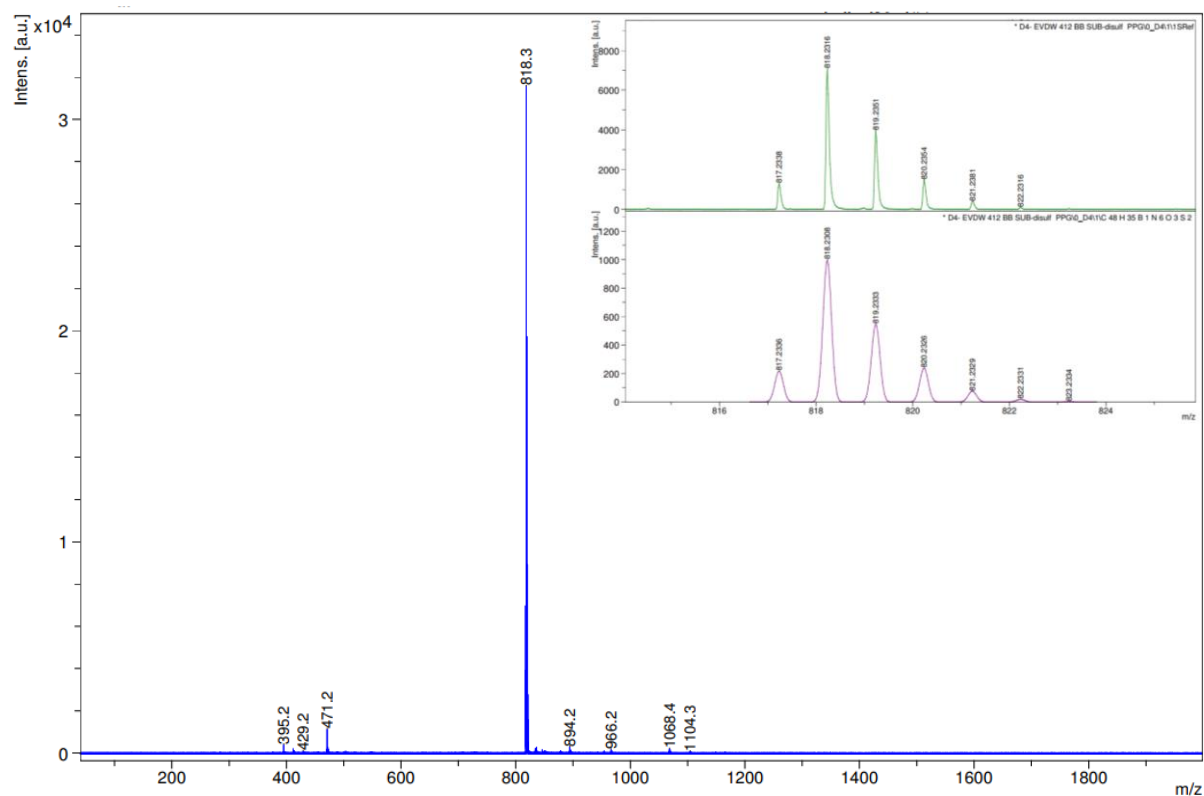
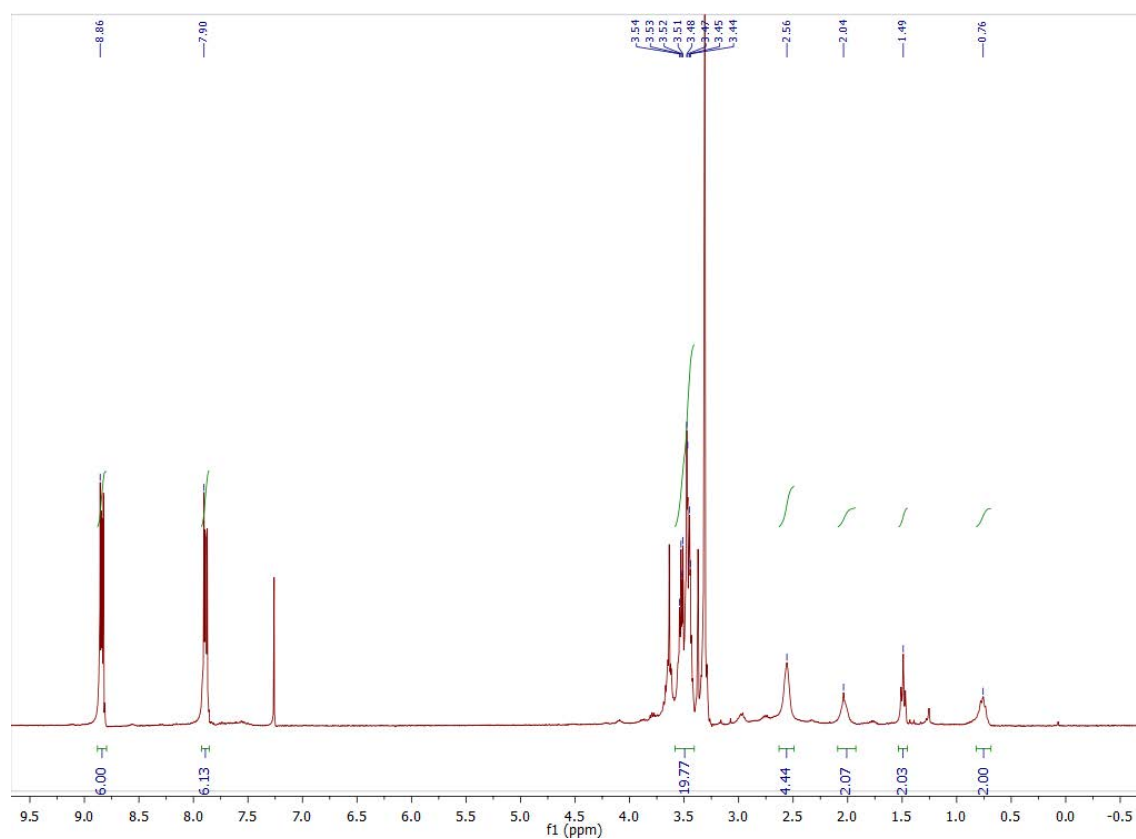
SubPc 1a. The title compound was obtained following the general procedure, using nucleophile **2** (0.16 g, 0.38 mmol) and toluene/THF (10:1) as the eluent. Further purification by SEC with Bio-Beads as the stationary phase and toluene as the eluent yielded compound **1a** (0.08 g, 52%) as a dark pink solid. Reaction time: 4 h. Mp > 250°C; ¹H NMR (300 MHz, CDCl₃, δ): 8.81 (dd, *J* = 5.9, 3.2 Hz, 6H; Ar H), 8.29 – 7.93 (m, 9H; Ar H), 7.83 (dd, *J* = 5.8, 3.2 Hz, 6H; Ar H), 4.06 (t, *J* = 6.5 Hz, 2H; CH₂), 3.36 (t, *J* = 7.6 Hz, 2H; CH₂), 2.48 (t, *J* = 6.5 Hz, 2H; CH₂), 2.40 (t, *J* = 7.1 Hz, 2H; CH₂), 2.16 (m, 2H; CH₂), 1.70 – 1.78 (m, 4H; CH₂); ¹³C NMR (75 MHz, CDCl₃, δ): 173.1 (C=O), 151.5 (C), 135.7 (C_{py}), 131.4 (C_{py}), 130.0 (C), 129.7 (CH), 129.0 (C_{py}), 128.7 (C_{py}), 128.2 (C_{py}), 128.3 (C_{py}), 127.8 (C_{py}), 127.5 (C_{py}), 127.0 (C_{py}), 126.9 (C_{py}), 126.2 (C_{py}), 125.3 (C_{py}), 124.5 (C_{py}), 124.4 (C_{py}), 123.9 (C_{py}), 122.9 (C_{py}), 122.1 (CH), 62.2 (CH₂), 57.7 (CH₂), 39.8 (CH₂), 37.1 (CH₂), 33.8 (CH₂), 32.8 (CH₂), 26.8 (CH₂); IR (ATR): ν = 1726 (C=O), 1455, 1381, 1285, 1171, 1128, 843, 731 cm⁻¹; UV-vis (DMF): λ_{\max} (log ϵ) = 562 (4.78), 544 (sh), 505 (sh), 344 (4.57), 327 (4.52), 311 nm (4.55); MALDI-TOF (DCTB) *m/z* (%): 1104.3 (2), 1068.4 (2), 966.2 (2), 894.2 (2), 818.3 (100) [M]⁺, 471.2 (5), 412.2 (2) [M-L_{axial}+OH]⁺, 395.2 (2) [M-L_{axial}]⁺; HRMS (MALDI) *m/z*: [M]⁺ calcd for C₄₈H₃₇BN₆O₃S₂, 818.2308; found, 818.2316.

SubPc 1b. The title compound was obtained following the general procedure, using nucleophile **3** (0.14 g, 0.38 mmol) and toluene/THF (10:1 to 1:1) as the eluent. Further purification by SEC with Bio-Beads as the stationary phase and toluene as the eluent yielded compound **1b** (0.06 g, 43%) as a dark pink sticky paste. Reaction time: 5 h. Mp > 250°C; ¹H NMR (300 MHz, CDCl₃, δ): 8.86 (dd, *J* = 5.7, 3.1 Hz, 6H; Ar H), 7.90 (dd, *J* = 5.8, 3.2 Hz, 6H; Ar H), 3.54 – 3.44 (m, 20H; CH₂), 3.35 (br s, 6H; CH₃), 2.56 (br s, 4H; CH₂), 2.04 (s, 2H; CH₂), 1.49 (t, *J* = 6.0 Hz, 2H; CH₂), 0.76 (br s, 2H; CH₂); ¹³C NMR (75 MHz, CDCl₃, δ):

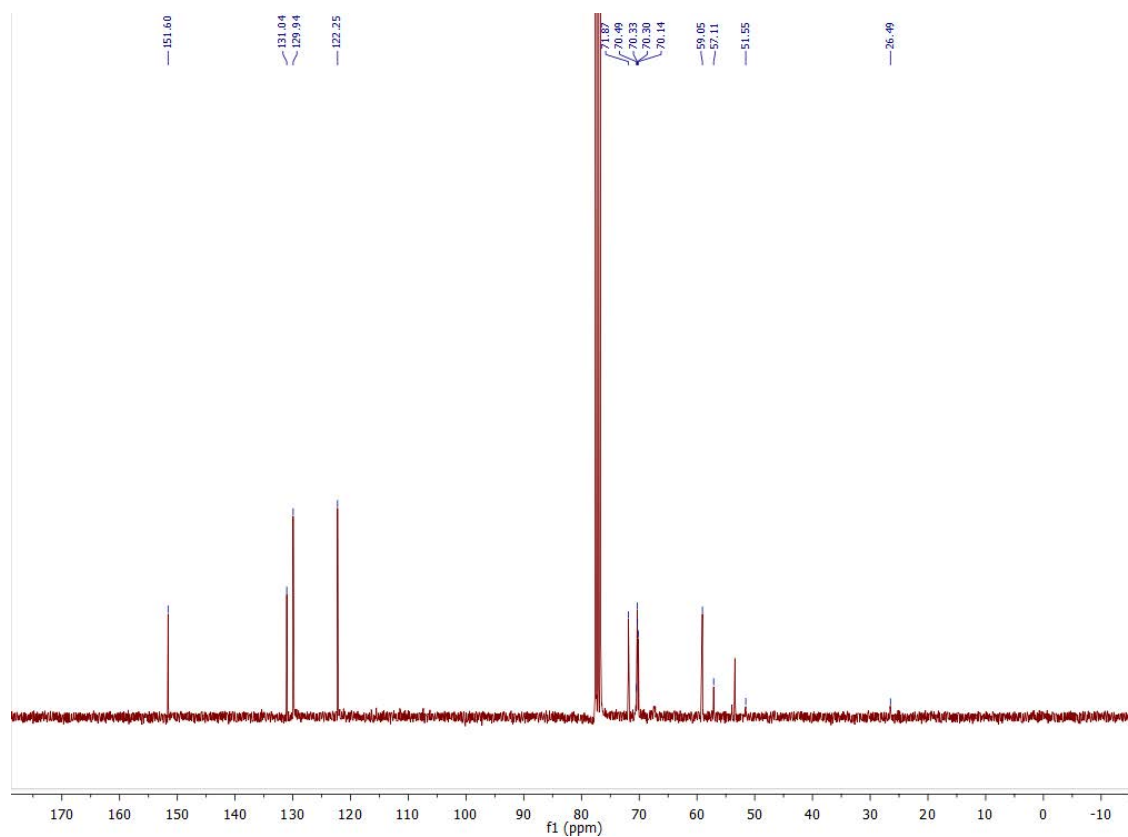
151.6 (C), 131.0 (C), 129.9 (CH), 122.2 (CH), 71.8 (CH₂), 70.3 (CH₂), 70.3 (CH₂), 70.1 (CH₂), 59.0 (CH₃), 57.1 (CH₂), 53.4 (CH₂), 51.5 (CH₂), 26.5 (CH₂); IR (ATR): $\nu = 2871$, 1725, 1465, 1376, 1284, 1249, 1090, 1028, 846, 744 cm⁻¹; UV-vis (DMF): $\lambda_{\max}(\log \varepsilon) = 562$ (4.97), 544 (sh), 506 (sh), 303 nm (4.70); APCI m/z (%): 818.3 (100), 762.4 (40) [M+H]⁺, 662.4 (30); HRMS (MALDI) m/z : [M+H]⁺ calcd for C₄₁H₄₈BN₇O₇, 762.3788; found, 762.3781.

SubPc 1c. The title compound was obtained following the general procedure, using nucleophile **3** (0.07 g, 0.38 mmol) and toluene/THF (30:1 to 10:1) as the eluent. Further purification by SEC with Bio-Beads as the stationary phase and toluene as the eluent yielded compound **1c** (0.07 g, 64%) as a dark pink solid. Reaction time: 3 h. Mp > 250°C; ¹H NMR (300 MHz, CDCl₃, δ): 8.86 (dd, $J = 5.8, 3.1$ Hz, 6H; Ar H), 7.90 (dd, $J = 5.9, 3.1$ Hz, 6H; Ar H), 4.02 (t, $J = 6.6$ Hz, 2H; CH₂), 2.47 (t, $J = 6.6$ Hz, 2H; CH₂), 1.99 (s, 3H; CH₃), 1.78 – 1.75 (m, 4H; CH₂); ¹³C NMR (75 MHz, CDCl₃, δ): 171.2 (C=O), 152.0 (C), 131.5 (C), 130.3 (CH), 122.6 (CH), 62.7 (CH₂), 58.2 (CH₂), 40.3 (CH₂), 37.5 (CH₂), 21.4 (CH₃); IR (ATR): $\nu = 1734$ (C=O), 1638, 1455, 1430, 1379, 1323, 1287, 1226, 1193, 1129, 1027, 738 cm⁻¹; UV-vis (DMF): $\lambda_{\max}(\log \varepsilon) = 562$ (4.86), 545 (sh), 507 (sh), 303 nm (4.59); MALDI-TOF (DCTB) m/z (%): 590.2 (100) [M]⁺, 471.2 (10) [M-(CH₂)₂OCOCH₃]⁺, 395.2 (5) [M-L_{axial}]⁺; HRMS (MALDI) m/z : [M]⁺ calcd for C₃₀H₂₃BN₆O₃S₂, 590.1366; found, 590.1385.

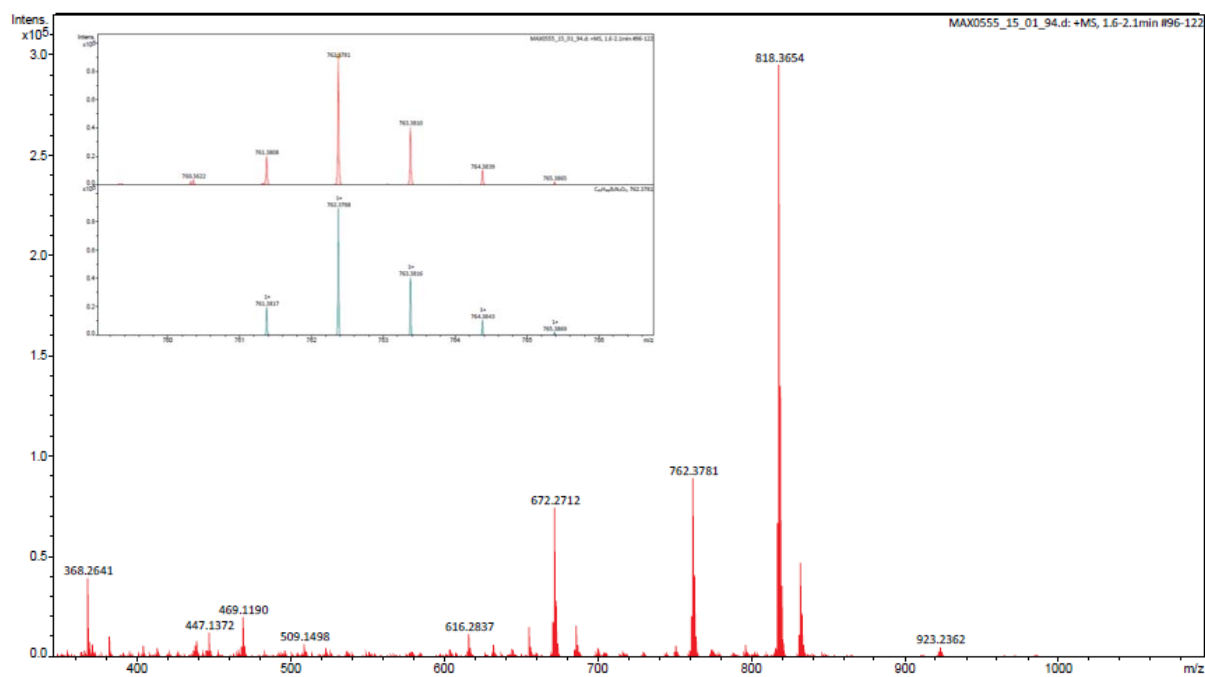
^1H NMR of SubPc **1a**: ^{13}C NMR of SubPc **1a**:

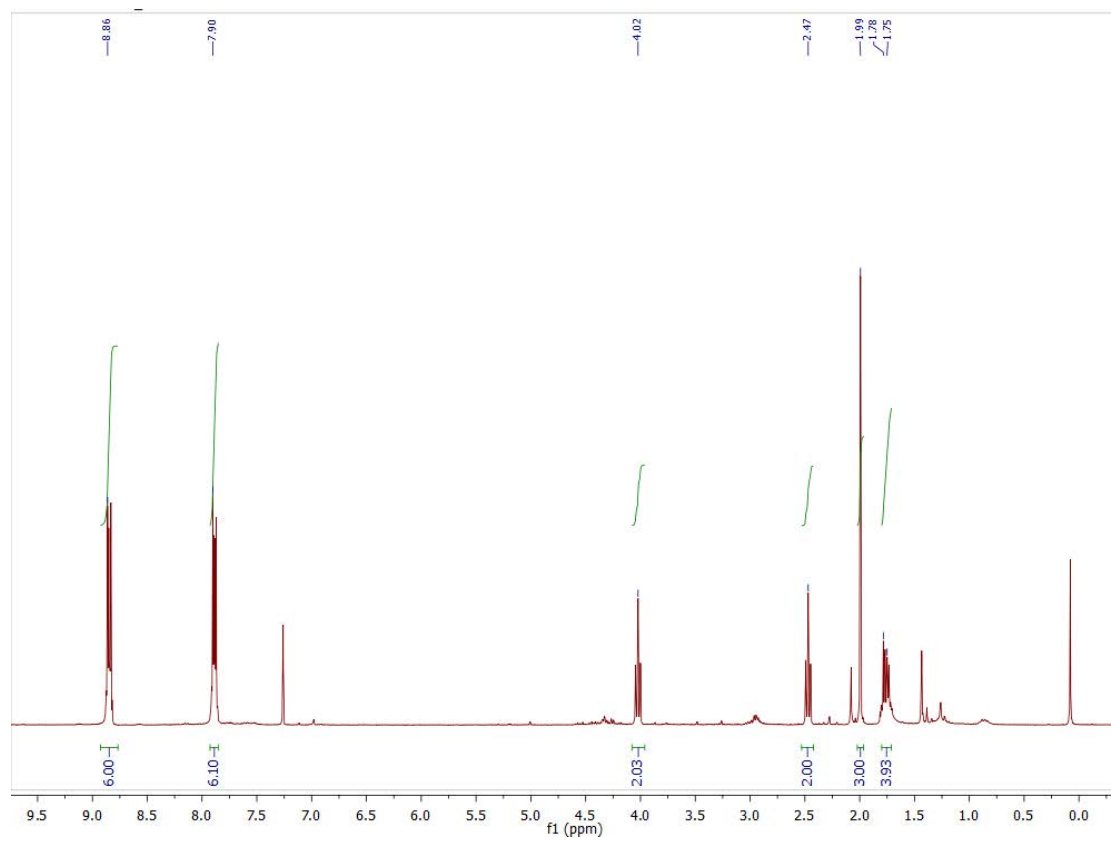
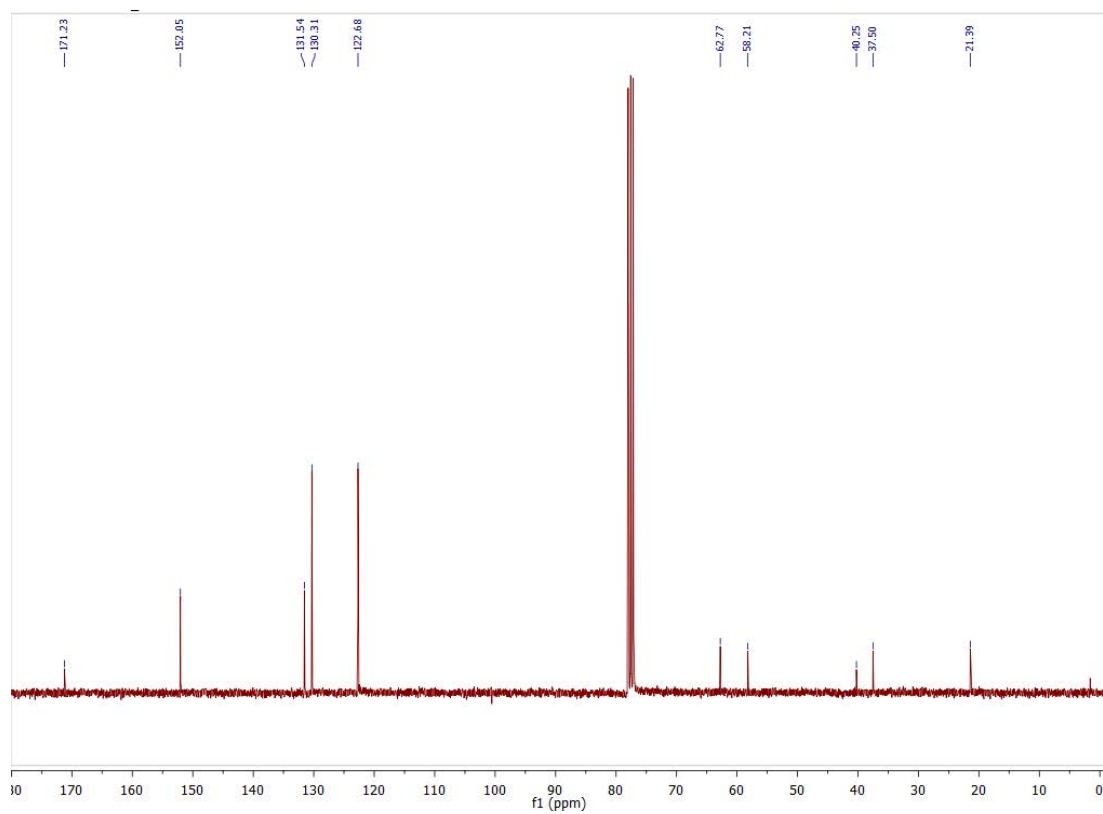
MS and HRMS (inset) analysis of SubPc 1a:¹H NMR of SubPc 1b:

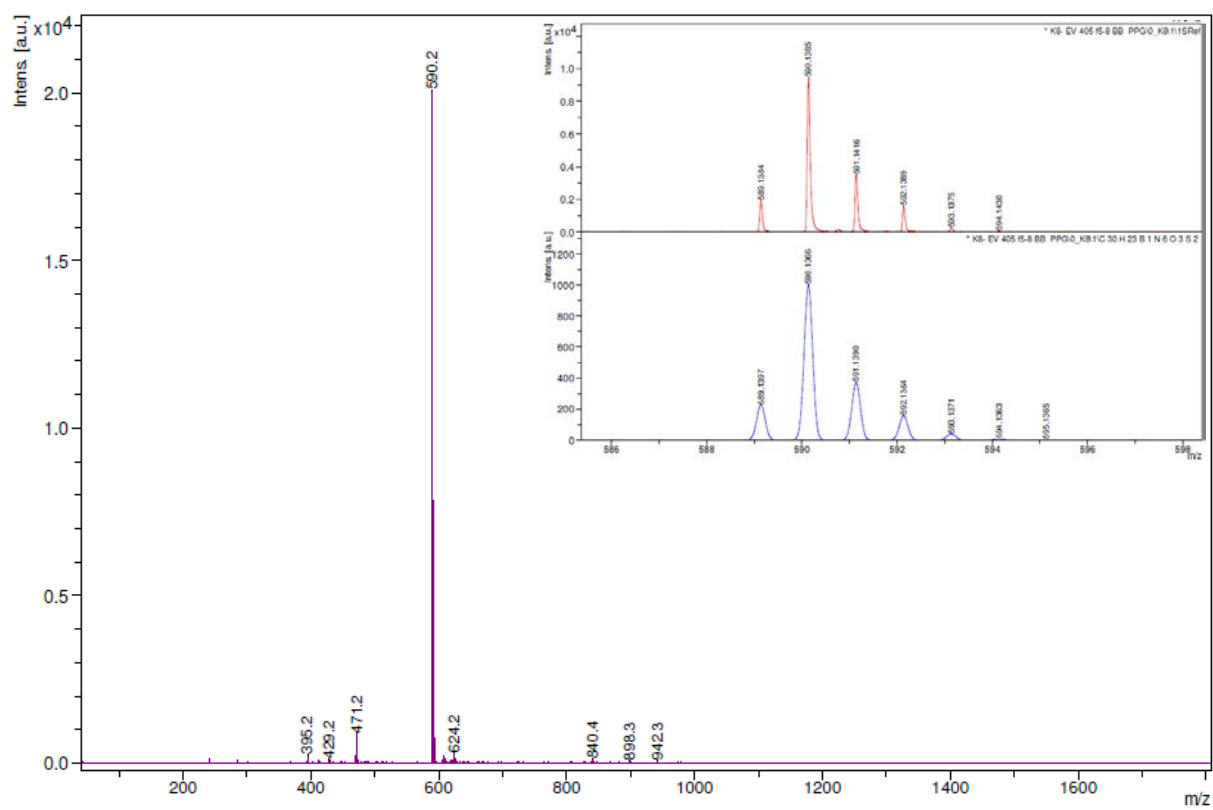
^{13}C NMR of SubPc **1b**:



MS and HRMS (inset) analysis of SubPc **1b**:



^1H NMR of SubPc **1c**: ^{13}C NMR of SubPc **1c**:

MS and HRMS (inset) analysis of SubPc **1c**:

4. References

- [1] A. T. R. Williams, S. A. Winfield, J. N. Miller, *Analyst* **1983**, *108*, 1067.
- [2] C. R. Nieto, J. Guilleme, C. Villegas, J. L. Delgado, D. González-Rodríguez, N. Martin, T. Torres, D. M. Guldi, R. S. Nohr, N. Martin, *J. Mater. Chem.* **2011**, *21*, 15914.
- [3] I. B. Berlman, *Handbook of Fluorescence Spectra of Aromatic Molecules*, Academic Press, New York, **1971**.
- [4] S. Makhseed, A. Tuhl, J. Samuel, P. Zimcik, N. Al-Awadi, V. Novakova, *Dye. Pigment.* **2012**, *95*, 351–357.
- [5] W. Spiller, H. Kliesch, D. Wöhrle, S. Hackbarth, B. Röder, G. Schnurpfeil, *J. Porphyrins Phthalocyanines* **1998**, *2*, 145–158.




Click here to access/download
Production Data
Figure 1.cdx











Click here to access/download
Production Data
Scheme 1.cdx

